THE DESIGN AND CONSTRUCTION OF AN ATOMIC FORCE MICROSCOPE

By

Emilie Ocock

A thesis submitted in partial fulfillment of the requirements for the degree of

Bachelor of Science

Houghton College

May 2014

Signature of Author…………………………………………..……………………..

Department of Physics
May 5, 2014

…………………………………………………………………………………..

Dr. Brandon Hoffman
Associate Professor of Physics
Research Supervisor

…………………………………………………………………………………..

Dr. Mark Yuly
Associate Professor of Physics

THE DESIGN AND CONSTRUCTION OF AN ATOMIC FORCE MICROSCOPE

By

Emilie Ocock

Submitted to the Department of Physics
on May 5, 2014 in partial fulfillment of the
requirement for the degree of
Bachelor of Science

Abstract

A variable temperature atomic force microscope (AFM) is being built at Houghton. The AFM will use a spring vibration isolation system with eddy current dampening in order to remove mechanical vibrations from both the machine and external sources. To approach and scan a sample, a modified "Johnny Walker" beetle will be built to move up, down, and across a ramp. Once complete and fully operational, this AFM will be able to scan samples on the resolution of nanometers, making it useful for many fields of science.

Thesis Supervisor: Dr. Brandon Hoffman
Title: Associate Professor of Physics

TABLE OF CONTENTS

Chapter 1: Introduction 2

1.1 The Atomic Force Microscope 2

1.2 History 2
1.2.1 AFM Predecessors 2
1.2.1.1 The Profiler 3
1.2.1.2 The Topografiner 3
1.2.1.3 The STM 4
1.2.2 The Origin of the AFM 5
1.2.3 The Current State of AFMs 6

1.3 Motivation and the Purpose of the Houghton AFM 7
1.3.1 Thin Films 7
1.3.2 Other methods of analysis 8

1.4 Previous Work on the Houghton AFM 9
1.4.1 Bethan Little's work 9
1.4.1.1 Initial designs 9
1.4.1.2 Variable temperature design 9
1.4.1.3 LabVIEW program 9
1.4.2 Optical input to LabVIEW 10
1.4.3 Current status 10

Chapter 2: Theory 11

2.1 Introduction 11

2.2 Cantilevers 11
2.2.1 Introduction 11
2.2.2 Cantilever Modeling 11
2.2.3 Forces 12
2.2.3.1 Capillary forces 12
2.2.3.2 Electrostatic forces 13
2.2.3.3 Lateral Forces 13
2.2.3.4 Van der Waals forces 13
2.2.4 The Lennard-Jones potential 15
2.2.5 Error from tip shape 16
2.2.6 Measuring Tip Movement 18
2.2.6.1 Optical Laser System 18

2.3 Methods of Operation 22
2.3.1 Contact Mode 22

2.3.2 Oscillating Mode 23
2.4 Piezoelectric Crystals 27
2.4.1 Piezoelectric Theory 28
2.4.2 Approach and Scan Theory 29
2.4.2.1 Expansion and contraction 29
2.4.2.2 Rocking motion 29
2.4.2.3 "Stick-slip" 30
2.4.3 Error Sources 30
Chapter 3: AFM Aparatus 33
3.1 Overall Model 33
3.2 Houghton Design 33
3.3 "Johnny Walker" Design 33
3.3.1 Sample Movement: Approach 35
3.3.2 Sample Movement: Scanning 36
3.4 Electronic Circuitry 38
3.4.1 Digital to Analog Circuitry 38
3.4.2 Piezoelectric Circuitry 40
3.5 LabVIEW Program 42
3.5.1 Output Program 42
3.6 Implementation 47
Chapter 4: Conclusion 48
4.1 Current Status 49
4.2 Future Work 49
4.3 Conclusion 50

TABLE OF FIGURES

Figure 1.1. Schematic of the profiler........ 3
Figure 1.2. Schematic of the topografiner 3
Figure 1.3. Schematic of the first AFM 4
Figure 1.4. Schematic of the STM 4
Figure 1.5. Schematic of common AFM designs 5
Figure 1.6. Comparison of current common microscopes 7
Figure 1.7. AFM topographic map of a $SrBi_2Nb_2O_9$ thin metal film 8
Figure 2.1. Tip interaction with contamination layer 12
Figure 2.2. Graph of the Lennard-Jones potential and force. 16
Figure 2.3. Schematic of showing the effect of different sized cantilever tips 17
Figure 2.4. Schematic of tip shapes that do not demonstrate a pointedness 18
Figure 2.5. Schematic of the optical laser detection system for an AFM 20
Figure 2.6. Schematic showing the change of angle ϕ and its effect on θ. 21
Figure 2.7. Schematics of the two methods of operations. 23
Figure 2.8. Schematics of the three modes of oscillation. 25
Figure 2.9. Expansion of a piezoelectric element 28
Figure 2.10. schematics of the three movements required of the piezoelectric tubes. 32
Figure 3.1. Schematic of the Houghton AFM 34
Figure 3.2. Images of the Houghton AFM Apparatus........ 35
Figure 3.3. Schematic of the piezoelectric tube movement under a triangle voltage 37
Figure 3.4. Schematic of the DAC circuitry 38
Figure 3.5. The timing diagram of the TLC5628C DAC 39
Figure 3.6. Diagram showing the geometry calculations for the approach circuit. 40
Figure 3.7. Scanning Circuitry 41
Figure 3.8. Approach Circuitry 42
Figure 3.9. Diagram of the saw tooth wave creation 43
Figure 3.10. Schematic of the DAC and the conversion to binary 45
Figure 3.11. Diagrams of the reordering array, clock array, and R/W array 46
Figure 3.12. Diagrams displaying the analog and digital outputs of the program 47
Figure 3.13. Schematic of the entire electrical circuit 48

Chapter 1

INTRODUCTION

1.1 The Atomic Force Microscope

The Houghton Atomic Force Microscope (AFM) will be used to make high resolution topographical maps of the surfaces of thin films in order to analyze their structures on the micrometer to nanometer scale. A cantilever tip scans across the surface of the film and interacts with it via atomic forces. These interactions are recorded to create a topographic map. Before discussing the theories and processes involved with the design and construction of the AFM, a brief history of the microscope will be given in order to demonstrate the motivation behind the machine being built at Houghton.

1.2 History

The history of microscopy, until the 20th century, was entirely comprised of optical microscopes – microscopes that require visible light to observe data. The maximum magnification of these "light" microscopes is roughly one thousand times. While this magnification was useful for basic observations that can be seen by the eye, it is hardly adequate for understanding how the sample behaves on a molecular scale. As a result, scientists began pushing the boundaries of microscopy and began to research alternative methods for analyzing samples on a molecular level. One of the significant byproducts of this research was the atomic force microscope which was developed in 1985 by Binnig, Gerber, and Quate [1]. While this was a significant advancement for the development of microscopy, it was not the only important microscope of that era and could not have been made without prior research being completed. There were several other advancements that were made before the conception of the AFM that had significant impacts on its research and functionality.

1.2.1 AFM Predecessors

The following are a few of the more notable instruments that were developed before and had significant influence on the creation of the AFM.

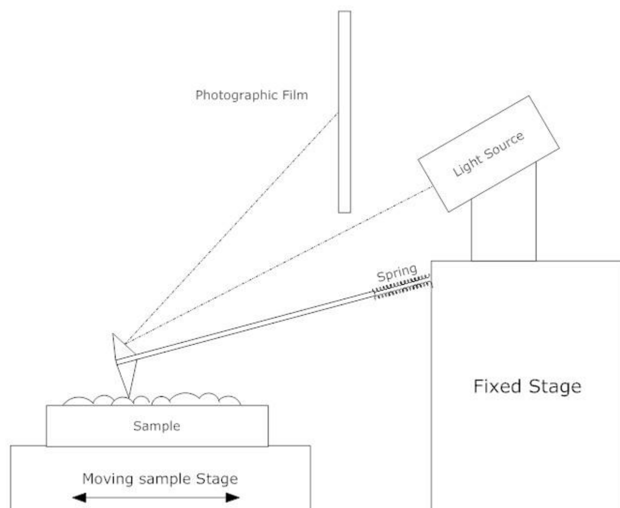

Figure 1.1. Schematic of the profiler. A sample would be positioned on a moveable sample stage. A probe attached to a fixed stage by a spring would scratch across the surface as the sample moves. As it is moving, a light source reflects off of a mirror on top of the probe and reflects onto a photographic film in order to make an image of the contours of the surface.

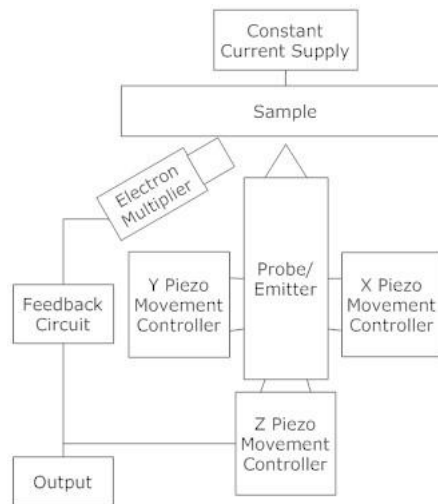

Figure 1.2. Schematic of the topografiner. The X and Y piezoelectric tube's movement controllers control the scanning process across the surface. The sample is given a constant current so that electrons can be detected off of the surface. This is done to keep a constant distance above the sample (since the distance is proportional to the amount of electrons detected). The output voltage is proportional to the distance in Z.

1.2.1.1 The Profiler

One of the first non-optical microscopes developed was the profiler. Invented in 1929 by the German engineer Gustav Schmalz [2,3], the profiler consisted of a cantilever tip that is scraped across the sample's surface – see Figure 1.1. As it was scanned, a light shown onto a mirror on the reverse side of the tip. The light would then reflect off of the tip onto a photographic film where the magnified image could be viewed. This process would create a magnified profile greater than one thousand times the original. There was a downside to this microscope though – the process of scraping across often damaged the sample and the tip where there were large features on the surface.

1.2.1.2 The Topografiner

The next significant advancement in the study of microscopy was that of the topografiner, invented in 1971 by Russell Young [4] (see Figure 1.2). This instrument built off the idea of the profiler in that it created a profile, but it did not scrape against the surface. Instead, the topografiner used the concept of

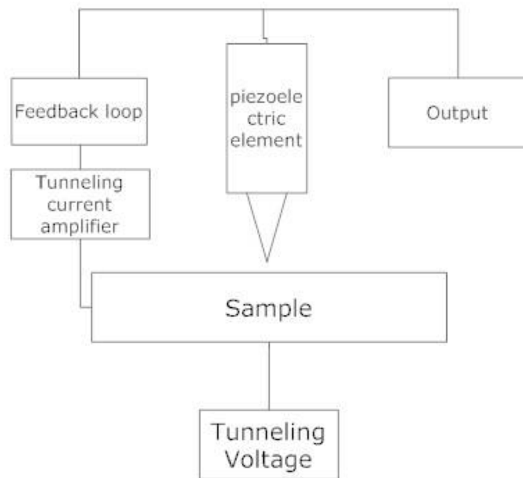

Figure 1.3. Schematic of the STM. The sample is charged with a constant current passing through it, so as it is scanned, the piezoelectric element and the tip create a tunneling current. The current is detected, amplified, and then sent into a feedback loop. It is kept constant by moving the tip up and down with the samples contours which is done by connecting the feedback loop to the piezoelectric element. The voltage required to move the tip-surface current constant is proportional to the distance, so that it the output.

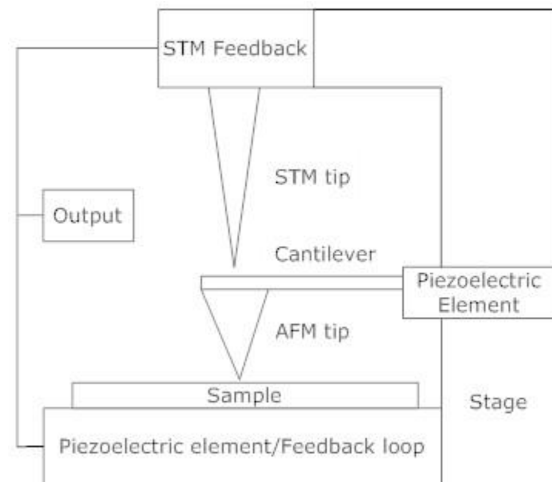

Figure 1.4 Schematic of the first AFM. The sample is scanned across by a diamond tipped cantilever that is controlled by a piezoelectric element. As it does this, it interacts with the atomic forces of the samples surface. These interactions are then detected by the STM tip that is interaction with the cantilever tip. The tunneling current is kept constant between the STM and the cantilever by moving the sample up and down as the sample is scanned. The output is proportional to the voltage required to move the sample and AFM tip at constant force.

electron field emission (EFE) to create a constant distance between the tip and the sample. EFE is the process of extracting electrons from a material using an electric field. Young was able to successfully scan on the resolution of 20 nm horizontal by 3 nm vertical. This maximum resolution was caused by weak distance dependence of the EFE current. The resolution was also limited by the vibrations caused by the machine and exterior noise.

1.2.1.3 The STM

The scanning tunneling microscope (STM), seen in Figure 1.3, was created in response to many significant improvements to the topografiner. Developed in 1982 by Binnig and Roher [5], the STM increased the resolution capabilities of microscopy by orders of magnitude and created a simpler method for making direct images of the atomic structure on the surface of a film. Unlike the topografiner, the STM was able to control the vibrations of the machine and avoid some of the exterior noise by making refinements to the overall design. The tip scans across the surface of the sample at distances close to one nanometer. It is important to note that this potential was on the order of one volt. This is less than the work function, meaning that by the classical model, the electrons would not be able to jump between

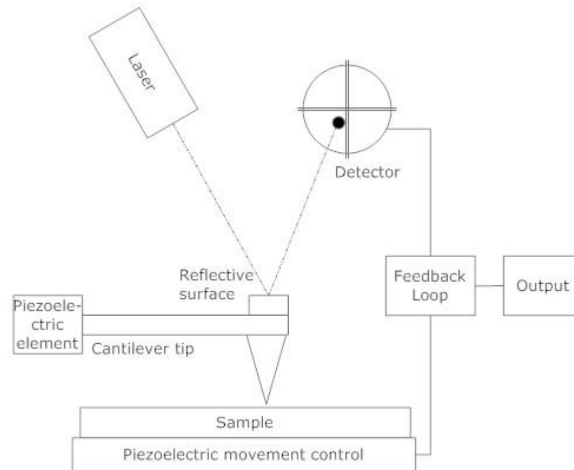

Figure 1.5. Schematic of common AFM designs. Here, the STM unit has been replaced with a laser optics system. As the AFM cantilever tip is driven by the piezoelectric element and interacts with the atomic forces of the sample, a laser reflects off of the back of the cantilever onto a quadrant detector. This data goes into a feedback loop that adjusts the sample to remain a constant distance from the tip (thus creating a constant force reading). The output is created from this information.

the tip and the sample. The principles outlined within quantum mechanics, however, allow for this to be possible. So, while scanning, the atoms on the tip interact with the electron cloud on the sample via a tunneling current. These interactions and tunneling current are proportional through an exponential dependence to the distance between the tip and the sample. As the tip moves closer to the sample by angstroms, the current increases in orders of magnitude. As a result, a topographic map can be created by using this relationship. The only downside to the STM is that a current between the tip and the sample must be present for the scan to be successful. Because of this, the sample must be conductive.

1.2.2 The Origin of the AFM

With the STM recently developed, many new applications of it as well as modifications began to form. In 1985, Binnig and Quate [1] developed the first AFM (seen in Figure 1.4). It was the combination of the basic principles of the STM along with the stylus of the profilometer. The initial resolutions of the machine were 3 nm laterally, and .1 nm vertically. The common issue with previous attempts at improvement was that the masses of the tips used to scan were too big to detect forces that can be as small as 10^{-18} N. Binnig and Quate solved this issue by using the STM to detect the movement of the

AFM tip since STMs were capable of detecting movement at that order of magnitude. Another improvement in the AFM was that it did not require the sample to be a conductive surface as the STM did.

The original AFM functioned as follows; it consisted of a cantilever with a stylus positioned between the sample and an STM tunneling tip, and was attached to a piezoelectric element that was used to drive the cantilever tip at the resonant frequency. The sample was attached to another piezoelectric element and feedback loop that were used to keep the atomic forces constant between the AFM tip and the sample by controlling the sample-tip distance as well as to scan across it. As the cantilever scanned across the surface, a feedback loop was used to keep a constant tunneling current between the STM tip and the cantilever. This was done by changing the force on the stylus. This method of data collection led to the possibility of detecting ridges of a sample with amplitudes lower than 0.1 nm.

1.2.3 The Current State of AFMs

Due to its accuracy and resolution, the AFM became a popular method of analysis to the point where they were commercially available for researchers. The overall concept of the AFM has not changed much between its inception and current models. The most significant change can be seen in the detection of force interactions (see Figure 1.5). Instead of using an STM to detect the change in the cantilever tip position, a laser optics system is used. The AFM cantilever tip is driven by the piezoelectric element and interacts with the atomic forces of the sample. A laser reflects off of the back of the cantilever onto a quadrant detector. This data goes into a feedback loop that adjusts the sample to remain a constant distance from the tip (thus creating a constant force reading). The output is created from this information.

In comparison to other significant microscopes that have been developed over the years, the AFM possesses some of the better resolution capabilities. It is able to reach resolutions as high as 10^{-10} m, a resolution only attainable by the transmission electron microscope (TEM), STM and itself – see Figure 1.6. The TEM, however, damages the surface of the sample it scans (since it hits it with a high energy electron beam) which makes sequential scans less and less accurate to the original state. As mentioned

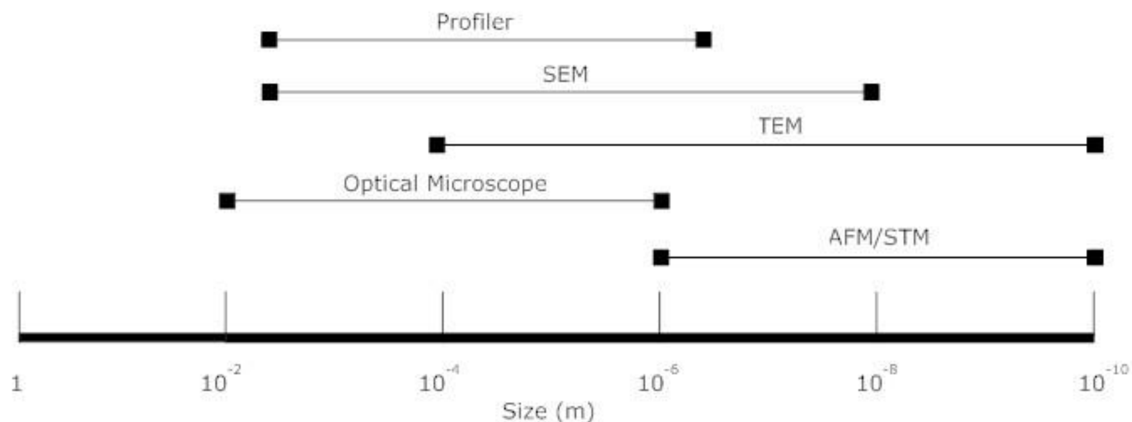

Figure 1.6. Comparison of current common microscopes. While the AFM does not have the range of some of the other modern microscopes, it is able to attain comparable resolution to many other methods on the small scale. It has the potential of a higher resolution than the scanning electron microscope (SEM), and has comparable resolution to the transmission electron microscope (TEM). Figure taken from Ref[2].

previously, the STM is able to only scan conductive or semi-conductive surfaces. The AFM, on the other hand, does not damage the surface and can scan almost any surface with features no larger than the scanning resolution capabilities (approximately 0.1 nm).

1.3 Motivation and the Purpose of the Houghton AFM

1.3.1 Thin Films

One of the focal points of research in the physics department at Houghton College is thin metal films. As the films are made, the material's atoms form a specific arrangement. This arrangement is repeated forming a pattern. The extents of this pattern form a crystal structure. Within a given sample, there are many different crystals with many different orientations with respect the surface of the film. Over time, the crystals with differing orientations can change if it is energetically favorable. This makes it important to analyze the films over a period of time. To do this, there are numerous possibilities, but it has been found that the AFM is a more than adequate technique for the analysis of thin films [6,7]. The use of AFM in observing surface morphology is now a common practice in the film research.

Due to the resolution capabilities, the AFM is able to detect different orientations of crystalline structures within a sample [8]. This can be done since the different orientations will have different surface structures. Figure 1.7 shows two AFM images taken by B. Gautier, et al. The images are primarily composed of a flat, dull orientation with spots of sharper, protruding orientations. While it is unable to identify which orientations are which, it is still beneficial to use the AFM for such a task, provided the tendencies of orientation changes are known. If the tendencies of crystal orientations and transformations are known, the samples structures can be analyzed and identified.

1.3.2 Other methods of analysis

Aside from the AFM, the Houghton College Physics department is currently working on the design and construction of three other instruments designed for the analysis of thin films. A deposition chamber is being constructed for the purpose of making thin films at specific thicknesses [9]. These films will then have the capability of being analyzed by an interferometer [10] *in situ* as well as by an x-ray diffractometer [11]. The AFM would give the department another dimension of analysis that would benefit the research possibilities. With these three tools for analysis, the film's thickness and stress can

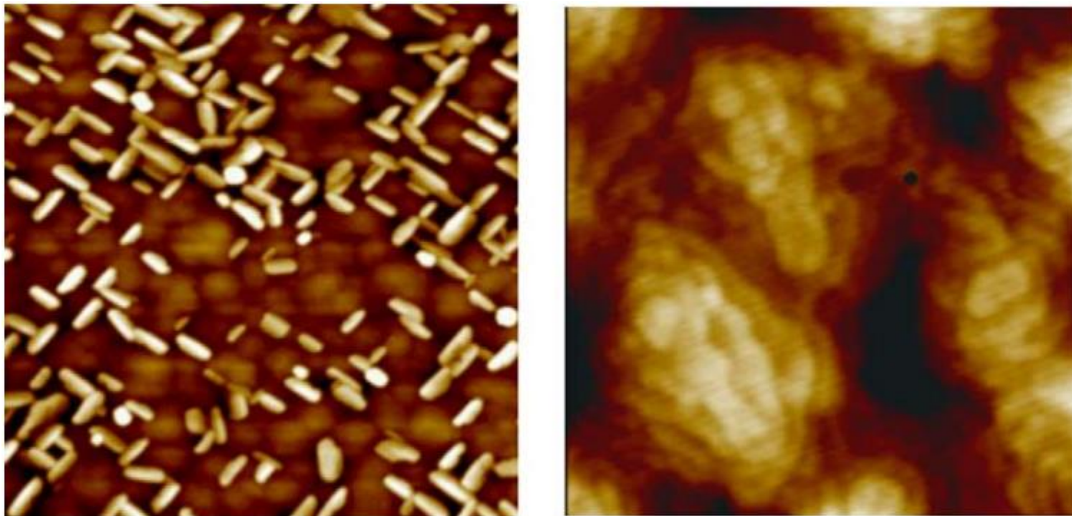

Figure 1.7. AFM topographic map of a $SrBi_2Nb_2O_9$ thin metal film. The left image is a 3μm × 3μm image of the film. Crystals of a specific orientation form the platelet-like grains that protrude from the flat background of another orientation. The right image is a 600nm × 600nm image of the flat background orientation crystals. Figure take from Ref[7].

be detected (via the interferometer), the volume percentages of the various significant crystalline structures can be recorded (via the diffractometer), and the surface features and crystalline formations can be detected as well as the potential of detecting their orientations (via the AFM).

1.4 Previous Work on the Houghton AFM

1.4.1 Bethany Little's work [21]

The work that is currently being done on the Houghton AFM is a continuation of a project that was started by a former student. Here is a brief overview of the work that was done.

1.4.1.1 Initial designs

The initial designs for the Houghton AFM were inspired from an AFM that was constructed in 1995 by Dai [12]. In these designs, the sample and tip are inverted from what would be considered normal positioning such that the tip scans the surface as it faces down. The sample is attached to a walker stage comprised of three piezoelectric tubes that descend and ascend a ramp to scan the surface of the sample. A dampening system is also used to remove the low frequencies of the building. The entire apparatus is suspended by a set of springs that are used to external vibrations. The cantilever tip will be oscillated by a small piece of piezoelectric ceramic that resides under the cantilever. It will be driven at the resonant frequency of the tip.

1.4.1.2 Variable temperature design

An attempt was made in previous designs to create a variable temperature capability for the Houghton AFM. The initial plan was to follow Dai *et al.* [8] in the design and use a cold finger (which uses liquid nitrogen to cool the sample) and resistive heating. The sample was isolated from the rest of the microscope for the purpose of removing thermal expansion issues. Varying the temperature, however, is not feasible with the current plans for the model. The temperature changes will affect the positioning of the sample and walker so much so that it will affect the actual results of the scans.

1.4.1.3 LabVIEW program

LabVIEW 8.2 was used as a programming environment to control the microscope. The program drives the piezoelectric tubes that move the sample and tip, reads the input from the laser optical detection

unit, and stores the data to create the topographic maps of the sample. Each of these tasks are in sub programs that are all called on in a simple user interface program. Work must be down on all three of these aspects as parts have been replaced and modifications have been made to improve the system.

1.4.2 Optical input to LabVIEW

One of the key aspects of the AFM is reading in the data from the optical laser detection unit. A focused laser beam must reflect off of the cantilever tip onto a quadrant detector in order to detect the movement of the probe. In order to be effective, the detector must be connected to a computer system that analyzes its data. The program used in the Houghton AFM is being written in LabVIEW. The original quadrant detector that was used was not very compatible to LabVIEW. It ran off of its own program and did not have an effective method to run in another program environment. To get around this, the detector was connected to another set of wiring in parallel to the other system. This was then run directly into the LabVIEW environment. Unfortunately, this did not work, as the setup caused an internal short circuit that ruined the input feed into the computer. A new detector has been purchased that is compatible with LabVIEW and should work for our AFM.

1.4.3 Current status

Upon the optical input failure and while awaiting the arrival of the new detector, current focus was shifted from there to the LabVIEW output and the unit that scans the sample across the cantilever tip. The output from the LabVIEW computer environment is a digital signal. This needs to be converted into a high voltage analog signal to operate piezoelectric tubes that operate the Johnny walker. The current status of the program and walker is being tested. A program and circuits have been made and now are currently being tested to move the sample stage.

Chapter 2

THEORY

2.1 Introduction

In order to successfully complete and construct a functional AFM, there are several important theories and ideas that must be well understood and applied. One of the most important theories is that of the cantilever and its probe tip, specifically, the forces acting on it and the probe tip. The common methods of operation for AFMs must also be considered. Finally, sources of error must also be accounted for in the topographic maps. This chapter gives brief theoretical descriptions of each of these topics needed for this machine's construction.

2.2 Cantilevers

2.2.1 Introduction

Due to its primary functions, the cantilever and its tip are arguably the most important part of the AFM and thus are the most important aspect to understand.

2.2.2 Cantilever Modeling

In recent years, researchers have become interested in effects of frequency in the response time of the cantilever tip. To better analyze them, a recent study modeled the cantilever and its probe based on four primary criteria: probe tip mass, cantilever beam deformation, and the rotary inertia of both the beam and the tip individually [13]. They concluded, however, that this model works best when the cantilever is much thicker in comparison to its length. If, on the other hand, it is thin in comparison to its length, a good model would be a simple harmonic oscillator. The Houghton AFM's cantilever will be modelled as a harmonic oscillator.

2.2.3 Forces

There are several important force interactions that occur between the tip and sample as it is scanned. The more prominent forces include capillary forces, electrostatic forces, and Van der Waals Forces.

2.2.3.1 Capillary forces

Since most AFMs operate at atmospheric pressure, there will almost always be a contamination layer at the surface [2] comprised of water and hydrocarbons. As a result, the tip is often surrounded by a contamination layer that can vary with sample and environment. Although it is generally uniform across the entire surface, the contamination layer can range in thickness from one to roughly fifty nanometers. This can lead to uncertainty in the actual measurements of the topography of the sample.

This contamination layer creates a force that needs to be considered in regards to the cantilever and its tip. When the cantilever is in contact with the contamination layer, the layer reshapes in the surrounding area to form a sort of neck (see Figure 2.1) that connects the probe to the to the surface. Since this interaction is hydrophilic, there is an attractive force between the tip and the sample. If the contamination layer is a constant thickness throughout the sample, the overall effect this causes will be minimal. It should be noted, however, that this layer will cause a general muddiness in the resolution

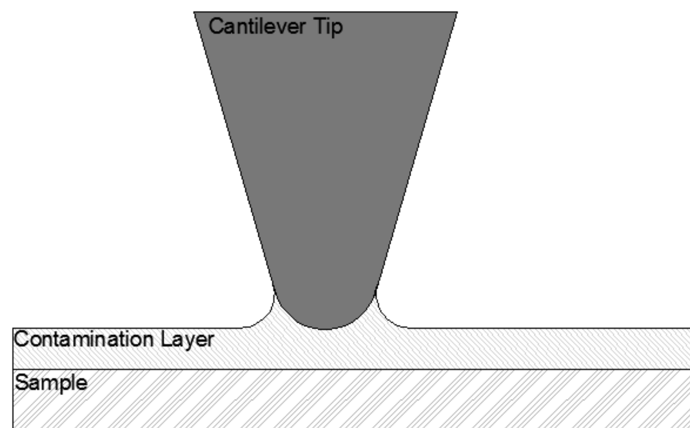

Figure 2.1. Tip interaction with contamination layer. Formation of neck between the cantilever tip and the contamination layer. Because the contamination layer-cantilever tip interaction is hydrophilic, there is an attractive force between the tip and the contamination layer.

that is dependent on its thickness. This is due to the fact that the layer will fill in the contours of the sample and as it does so, it will not form a completely even coating throughout.

2.2.3.2 Electrostatic forces

The electrostatic forces that are present in the scanning process are some of the larger intermolecular forces involved [14]. As the tip approaches the sample, it will potentially have a different charge than the sample. This is because the net charge on both the cantilever and the sample are independent of one another. By Coulombs Law, this force is proportional to $\frac{1}{r^2}$ and is written as the following:

$$F = \frac{1}{4\pi\varepsilon_0}\frac{q_t q_s}{r^2} \tag{2.1}$$

where ε_0 is a constant, q_t is the charge on the tip and q_s is the charge on the sample, r is the separation between them. This relationship will either cause a repulsive or attractive force, depending on the sign of q_t and q_s. This attractive or repulsive force can cause the resolution of the sample to be muddied slightly.

2.2.3.3 Lateral Forces

When the tip is in constant contact with the sample as it scans, which occurs in contact mode (see section 2.3), there are some lateral forces that occur on the cantilever and its tip. These forces are primarily caused by, though not limited to, the frictional component of the net force as the tip is dragged across the surface of the sample. These forces can cause rotations and twisting in the cantilever beam. This can be avoided for the most part if the tip does not drag across the surface but rather taps the surface (see section 2.3).

2.2.3.4 Van der Waals forces

The Van der Waals forces (VDW) between the sample and the cantilever tip are one of the primary force interactions that occur during the approaching and scanning processes. These VDW interactions are caused by a change in the dipole moment that comes from a shift of orbital electrons to one side of an atom or molecule. This shift, in turn, causes a similar action to occur in neighboring particles [15].

As a result, there can be interactions between any given number of atoms and molecules including neutral elements [16]. Because this is not limited to one direction, VDW forces can be both repulsive and attractive. It has been found that VDW forces are attractive for like materials, while it can be repulsive with some combinations of different materials. Interactions between two molecules can be affected by the introduction of a third molecule. Thus within a body of molecules, a single particle will interact with each and every other particle in the system. As a result, the sum of all interactions cannot be calculated by adding the sum of individual pair interactions. These interactions, however, will become less important proportionally to $\frac{1}{r^n}$ where *r* is the distance between the two particles and *n* is dependent on the range of *r*.

The energy between two particles due to the VDW interactions has been calculated [15] to be

$$E_{VDW} = -\frac{\pi^2 C \rho_t \rho_s R}{6r^{6-m}}, \tag{2.2}$$

where *m* is a constant. Specifically, the energy between a sphere (which is a good approximation for the tip of the probe) and a flat surface is given by:

$$E_{VDW} = -\frac{\pi^2 C \rho_t \rho_s R}{6r} \tag{2.3}$$

where *R* is the radius of the sphere (tip) and ρ_t and ρ_s are the number of atoms per unit volume in the tip and sample, respectively. *C* is the coefficient of the atom-atom pair potential. This method ignores the effects of the adjacent bodies which can make it difficult to accurately find this value if there is another body involved (i.e. the contamination layer).

In order to calculate the VDW force between the tip and the sample at a given point in time, the geometry of both must be examined as the molecules in each are arranged in a specific pattern. As mentioned previously the VDW force should be modeled between a sphere and a plane. Alternatively, it has been found that if it is modeled instead as two spheres where one of the spheres is has an infinite

radius, the force calculated will be equivalent to a sphere-plane system [17]. By using this system, the energy between the two spheres is found to be:

$$E = -\pi^2 \rho^2 \lambda \frac{1}{12r} \tag{2.4}$$

for $r \ll 1$ where λ is the VDW constant. Taking the derivative of this leads to the VDW force

$$F = \frac{\pi^2 \rho^2 \lambda}{24R} \frac{1}{r^2}. \tag{2.5}$$

2.2.4 The Lennard-Jones potential

The Lennard-Jones potential (LJP) is an approximation of the sum of the forces involved in the interaction between a pair of neutral particles. This potential and the force that comes from it lead to some interesting characteristics within the tip-sample interactions as it causes repulsion at short ranges (up to roughly 3 Å) [18] and attraction at long range (via the van der Waals potential described in the preceding section). This repulsive potential can be mathematically described as follows:

$$E(r) = \left(\frac{\sigma}{r}\right)^n, \tag{2.6}$$

where σ is the finite distance at which the inter-particle potential is zero and r is the distance between the two particles. The LJP is comprised of this potential as well as that of the VDW potential, which then gives us

$$E(r) = 4V_0 \left[\left(\frac{\sigma}{r}\right)^{12} - \left(\frac{\sigma}{r}\right)^6\right], \tag{2.7}$$

where V_0 is the depth of the potential well. This, however, is the energy between two molecules (recall equation 2.2). It has been found that for an interaction between the cantilever and a sample, m is equal to 5. This gives us a new energy of

$$E(r) = 4V_0 \left[\left(\frac{\sigma}{r}\right)^7 - \left(\frac{\sigma}{r}\right)\right] \tag{2.8}$$

The LJP can be converted into a force by taking the derivate and obtaining

$$F(r) = 24V_0\left[\left(\frac{\sigma}{r^2}\right) - \frac{\sigma^{12}}{r^{13}}\right]. \tag{2.9}$$

Figure 2.2 displays a graph of how this potential and force behave with respect to the separation.

2.2.5 Error from tip shape

The shape of the end of the cantilever tip can have a significant impact on the final topographic image of the sample. In fact, it can be one of the limiting factors in the final resolution of the image. If the tip is significantly smaller than the facets on the surface of the film, then this issue will be minimal and optimum resolution will be achieved.

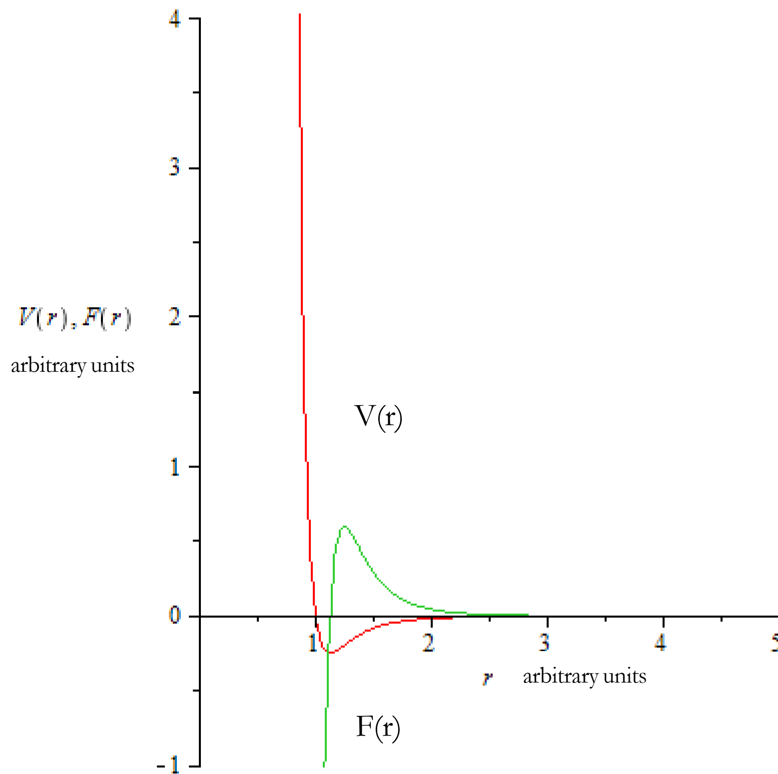

Figure 2.2. Graph of the Lennard-Jones potential and force. Here, $V_0 = \frac{1}{24}$ and $\sigma = 1$. It is evident that there are short and long range effects caused by this model.

In order to avoid this important issue, an optimal probe shape must be chosen for ideal scanning. To decide on the optimal shape, there are several aspects of the tip shape error that must be considered: facets appearing too small or large, abnormalities in the geometry, and repeating patterns. Figure 2.3 shows a schematic of the paths of different shaped cantilever tips. As can be seen, it is evident that the smallest tip gives the most accuracy in terms of both depth and width. A tip with an infinitesimal angle, however, would still not be the most ideal probe. If, instead of a pointed tip, there was a "T" shape, then it would be theoretically possible to map the inlets under the certain shaped facets. This phenomenon can be seen in Figure 2.4. By having a "T" shaped cantilever tip, it would be possible to map some of the smaller undercuts of the surface geometry. This concept of a "T" cantilever tip, however, does not fit into the current plan for the Houghton AFM. In order to accommodate a "T" tip and be able to scan without damaging it would require significant changes to the scanning process.

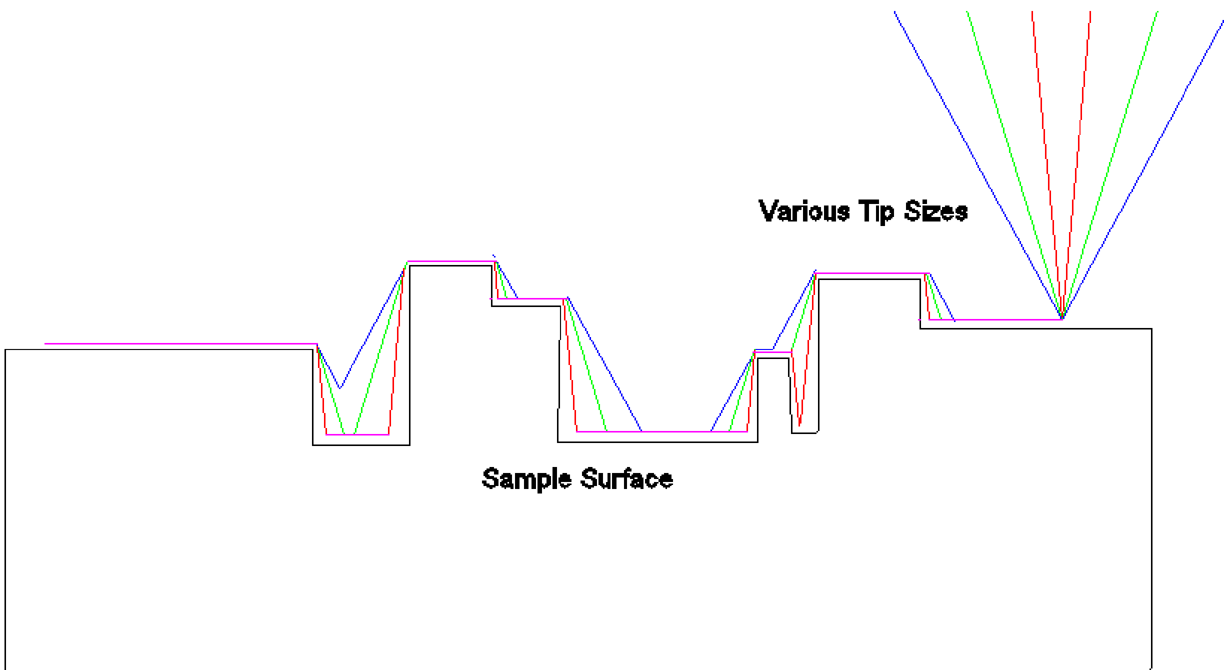

Figure 2.3. Schematic of showing the effect of different sized cantilever tips. The paths that are shared are shown in pink, while the differing paths are show for the different tip sizes. It can be see that as the angle of the point approaches 0, the topographic map would approach peak accuracy. Note that this does not include abnormal shapes or cave-like facets.

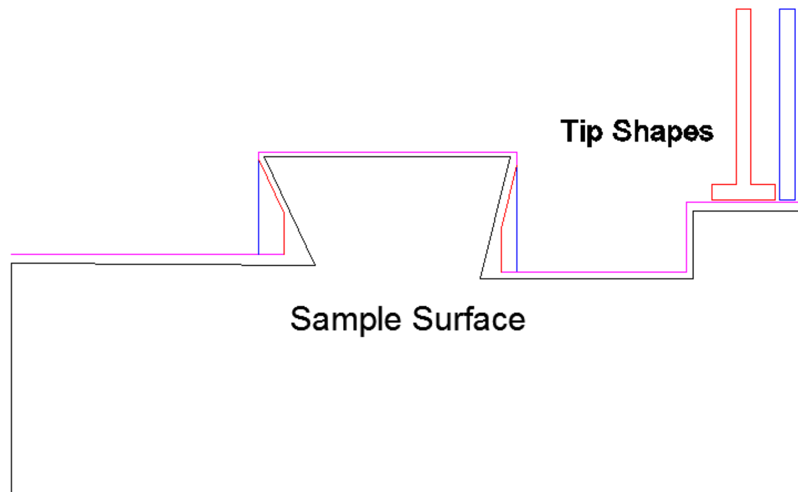

Figure 2.4. Schematic of tip shapes that do not demonstrate a pointedness. If a "T" shaped tip could be fabricated accurately, then it would be feasible to create images capable of detecting undercuts to the facets (observe the red path).

A pointed tip despite the inaccuracies demonstrated is more than adequate for most analytical processes involving thin films.

2.2.6 Measuring Tip Movement

The original AFM in 1985 had significant similarities to the STM of that era. In fact, in order to track the tip movement, an STM probe was used. As the AFM tip scanned across an insulating surface, the STM would track the movement of the cantilever which was made out of a conductive surface. While this was ingenious at the time, it has since become an outdated way of measuring the movement of the cantilever probe. Now, modern AFMs detect tip movement by using an optical laser system.

2.2.6.1 Optical Laser System

The most common method for tracking tip movement is through the use of a focused optical laser and a quadrant laser detector. The laser beam reflects off of a reflective coating on the back of the cantilever tip and up onto the quadrant detector. As the tip scans the surface, it will move up and down and at times rotate. All of these movements can be tracked by the optical laser system. This system works much more effectively than the original method (i.e. the STM tip) as it removes any potential for

additional forces acting on the cantilever tip since the laser does exert a substantial force when it reflects. The system can be observed in Figure 2.5.

Additionally, the resolution of the optics can be calculated by the following. To do so, first the angle the cantilever bends must be calculated. The amount something curves is proportional to the bending moment applied:

$$M = EI\kappa = \frac{EI}{r} \tag{2.10}$$

where *M* is the moment about the fixed end of the cantilever, *I* is the moment of inertia of the cantilever, *E* is a Young's Modulus, κ is the curvature, and *r* is the radius of curvature. By using this and the fact that

$$\kappa = \frac{d\phi}{ds}, \tag{2.11}$$

the following expression can be obtained:

$$\frac{M}{EI} = \frac{d\phi}{ds} \approx \frac{d\phi}{dx}, \qquad \phi \ll 1 \tag{2.12}$$

where ϕ is the angle the cantilever has bent, and *s* is the arc length of the cantilever. If ϕ small, s can be approximated to x, the dimension along the unbent cantilever. For these calculations, let $x = 0$ at the cantilever support, and $x = X$ at the location of the tip. If M is solved for from the integral relationship,

$$\Delta M = -\int V\, dx\,, \tag{2.13}$$

where V is the shear force. Since the only external forces on the cantilever support are at one end and the force interaction between the tip and sample, called F, V will be constant throughout the length of the cantilever and also equal to F. From this, the following is calculated:

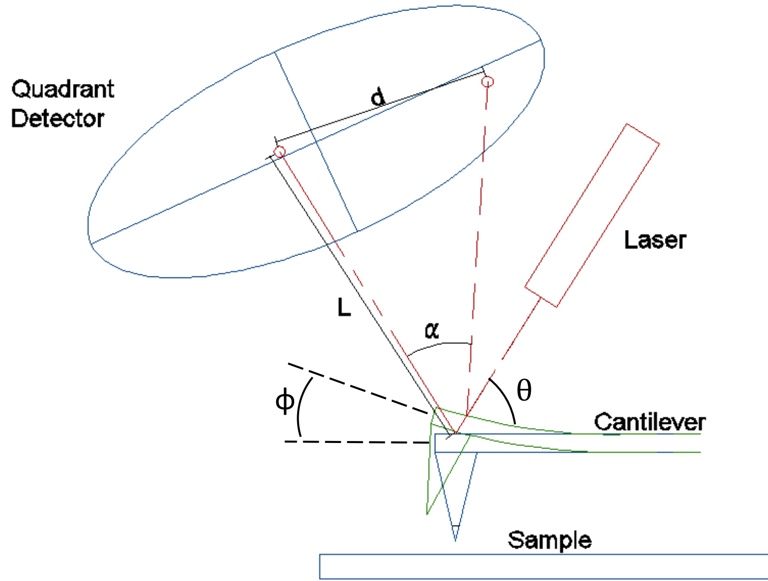

Figure 2.5. Schematic of the optical laser detection system for an AFM. Here, the laser reflects off the back of the cantilever tip and onto a quadrant detector. The movement of the laser beam on the quadrant detector is proportional to the movements of the tip against the sample surface. As the tip is twisted and pushed up and down by the forces involved, all of these will be recorded by the quadrant detector and relayed to a computer system.

$$M = M_0 - Fx = F(X - x) \tag{2.14}$$

where M_0 is the moment about the origin. It is found by requiring that the bending moment be equal to 0 at the tip side of the cantilever. F is the summation of all the forces interactive between the sample and tip, and $X$is the total length of the cantilever. From this, and assuming that the bending angle will be small, it can be deduced that

$$\phi = \frac{F}{EI}\left(Xx - \frac{x^2}{2}\right) \tag{2.15}$$

which can be simplified when x=X

$$\phi_{x=X} = \frac{F}{2EI}X^2. \tag{2.16}$$

It is now important to note that

$$\tan\phi = \frac{dz}{dx}, \tag{2.17}$$

but if a small angle approximation of $\tan\theta \approx \theta$ is made, we can further simplify this by solving for *dz*.

$$dz \approx \phi dx = \frac{F}{EI}\left(Xx - \frac{x^2}{2}\right)dx. \tag{2.18}$$

To solve for *Z*, integrate and obtain:

$$Z = \int_0^X z\,dx = \frac{F}{3EI}X^3 \tag{2.19}$$

where Z is the total bending motion in the Z axis. This can then be used in conjuncture with equation 10 to solve for ϕ in just terms of *X* and *Z*

$$\phi_{x=X} = \frac{3}{2}\frac{Z}{X}. \tag{2.20}$$

This angle is the primary factor that affects the angle of reflections change. Figure 2.6 describes how ϕ affects θ and thus the position of the beam on the detector. As the cantilever bends due to the external forces, ϕ will increase which causes θ to also increase. Because of this the angle of reflection will also

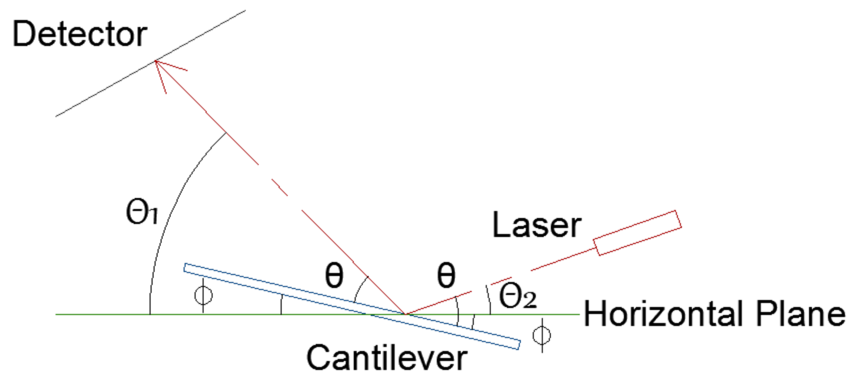

Figure 2.6. Schematic showing the change of angle ϕ and its effect on θ. As ϕ increases, θ increases causing the reflections position on the detector to change proportionally to 2θ.

decrease which will move the position of the beam on the detector. To calculate the distance it moves on the detector (and therefore the maximum resolution of the detector), note that

$$\Theta_2 = \theta - \phi \, , \tag{2.21}$$

and

$$\Theta_1 = \theta + \phi = \Theta_2 + 2\phi. \tag{2.22}$$

From this we can see that the angle moved can be calculated to

$$\alpha \equiv \Delta\Theta_1 = 2(\Delta\phi). \tag{2.23}$$

If the distance between the reflection point and the original point of contact on the detector is known (let it be called *y*), then the distance the laser moves on the detector can be found as:

$$d = L \tan \alpha \approx L\alpha = 2L(\Delta\phi) = \frac{3L}{X}(\Delta Z). \tag{2.24}$$

From this, it can be seen that the resolution of the movement in the Y-direction is directly proportional to the distance between the original reflection off of the cantilever and the detector. The larger the distance, the higher resolution can be attained.

2.3 Methods of Operation

The process of scanning can be completed by two primary modes of movement within an atomic force microscope. The following will give a brief overview of these different modes and some of the important differences that lead to different results within scans.

2.3.1 Contact Mode

The contact mode of scanning involves the tip being moved across the surface of the sample (see Figure 2.7 (a)). As it moves across, it is kept at a constant force (and therefore the distance between the sample and the surface remains the same) through a feedback loop. This loop is then used to create a topographic map of the surface. Despite its simplistic form, there are some major drawbacks to this mode of operation. Since the probe is being scraped across the surface of the sample, there can be significant damages to both the tip (complete destruction) and the sample (significant gouges and scratch

marks). The resolution of this method of scanning is equal to the resolution of the optics system. This is because the tip moves up and down with the sample surface.

2.3.2 Oscillating Mode

The oscillating mode of scanning (seen in Figure 2.7 (b)) is much more complicated than the contact mode of scanning but eliminates the potential of damaging the sample and the probe. In this mode, the cantilever and its tip are set to move at a resonant frequency. As the tip is moving at its resonant frequency, it comes close to the surface of the sample. When it does this, the sample and tip interact with each other through the interaction forces mentioned previously which causes a disturbance in the resonant frequency. In order to keep this frequency constant, however, either the cantilever or the sample must move up or down. As this movement occurs, it is recorded to create the topographic map of the surface.

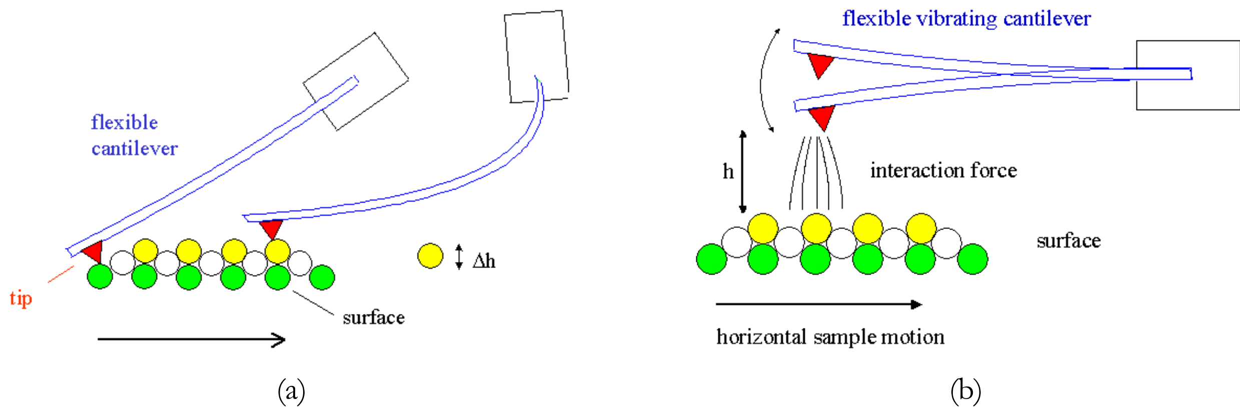

Figure 2.7. Schematics of the two methods of operations. Figure 2.5 (a) displays the contact mode where the cantilever and its tip scrape across the surface of the sample. As it does so, the tip moves up and down. This movement is detected and is converted into a topographic map. Figure 2.5 (b) displays the oscillation mode. In this mode, the cantilever is oscillated at its resonant frequency. As it nears the sample the tip interacts with the surface which affects the frequency the tip is being driven at. This adjustment is detected and sent into a feedback loop which then converts it into a topographic map.

While this mode is more complex that the contact mode, it can be more effective as there are various settings that can be altered to create sub-modes that give different informative scans about the sample surface. These different modes create different results in regards to the contamination layer.

In the first of these sub-modes the cantilever probe oscillates across the surface of the contamination layer in an attempt to vary the methods of scanning (see Figure 2.8 (a)). For this, the amplitude of oscillation must be small and the cantilever must have a lower resonant frequency (higher spring constant). This is so that the probe will not penetrate the surface of the contamination layer. The resolution of the scan in this mode is much lower in comparison to the other two sub-modes, appearing cloudy. This is primarily caused by the contamination layer filling the surface structures on the sample.

In the second of these sub-modes, the cantilever oscillates in just the contamination layer. Because of this, however, very high resolutions can be achieved. Here, the tip scans within the contamination layer of the sample but does not touch the sample itself (see Figure 2.8 (b)). In order to work, the cantilever must be fairly stiff with a very small amplitude in the resonant frequency. This is so that the tip does not jump back up above the contamination layer.

In the third and final sub-mode, the probe is oscillated in and out of the contamination layer (see Figure 2.8 (c)). The energy within the oscillating cantilever is much larger than in the other modes as the amplitude must be greater so as to move in and out of the contaminating layer. The energy is also greater than the capillary forces that prevent the other modes from penetrating the contamination layer as effectively. As a result, it is able to enter and exit this layer with ease as it scans. Because of this higher energy, however, there is much more risk in damaging the sample or the cantilever tip since the tip often crashes into the sample surface. It is, however, the easiest of these three sub-modes to implement.

In order to find a general resolution of these different oscillating modes, it is important to look at the mechanics of a damped harmonic oscillator [19,20]. The cantilever will be driven by an external oscillator that can be described with the following equation:

$$F(t) = F_0 \cos \Omega t \tag{2.25}$$

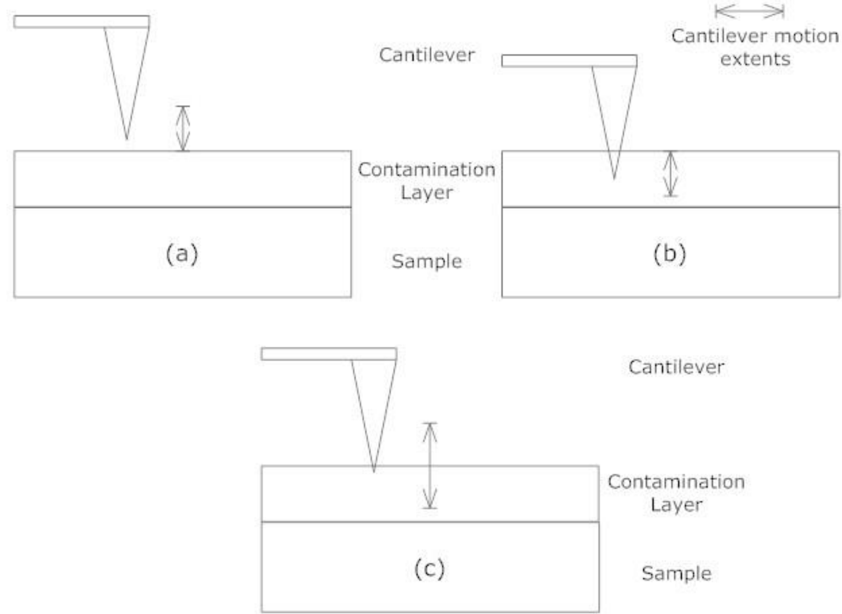

Figure 2.8. Schematics of the three modes of oscillation. In the first mode (a), the tip only oscillates on the surface of the contamination layer. This gives a much cloudier resolution. In the second mode (b), the cantilever only oscillates in the contamination layer. This method yields the best resolutions per image but is significantly harder to achieve. In the third mode of scanning (c), the probe oscillates both outside and inside the contamination layer. The resolution of these images are typically in between methods (a) and (b) and is significantly easier to achieve than (b).

where A is the amplitude of the force applied and Ω is its frequency. If the cantilever does not experience any external forces, the equation of motion can be found to be

$$\ddot{z} + {\omega_0}^2 z = \frac{F_0}{m}\cos\Omega t. \qquad (2.26)$$

This can then be solved to get the solution of

$$z(t) = \left(\sqrt{\left(x_0 - \frac{F_0}{m({\omega_0}^2 - \Omega^2)}\right)^2 + \left(\frac{v_0}{\omega_0}\right)^2}\right)\cos(\omega_0 t + \phi_0) + \left(\frac{F_0}{m({\omega_0}^2 - \Omega^2)}\right)\cos\Omega t \qquad (2.27)$$

where x_0 is the equilibrium position, ϕ_0 is the phase shift of the oscillations, v_0 is the initial velocity, and ω_0 is the resonant frequency which is

$$\omega_0 = \sqrt{\frac{k}{m}}. \tag{2.28}$$

The first portion of this solution describes the free oscillations, while the second describes the oscillations that are of the cantilever caused by the external force. From this it can be seen that the driving force is not the sole condition for the oscillations. The conditions prior to the external force must also be considered.

For the case of a cantilever oscillating in a force field with friction dampening the oscillations, the equation of motion of the tip can be described as:

$$\ddot{z} + 2\delta\dot{z} + {\omega_0}^2 z = \frac{F_0}{m}\cos\Omega t + \frac{F(z)}{m} \tag{2.29}$$

where δ is the damping factor, $\omega_0$is the resonant frequency, $\frac{F_0}{m}$ is the amplitude of the driving frequency, Ω is the driving frequency, m is the mass of the cantilever, and $F(z)$ is the sum of the forces on the tip from the sample and its action on the cantilever leads to a change in the equilibrium position of the oscillations. $F(z)$ can be approximated for small oscillations by taking the Taylor series at the point z_0, the equilibrium position.

$$F(z) = F(z_0) + \frac{dF(z_0)}{dz}\acute{z}(t) + \cdots, \tag{2.30}$$

where

$$\acute{z}(t) = z(t) - z_0, \tag{2.31}$$

and z_0 is derived by

$${\omega_0}^2 z_0 = \frac{F(z_0)}{m}. \tag{2.32}$$

By using Equations 17-20, a new equation of motion can be written as

$$\acute{\ddot{z}} + 2\delta\acute{\dot{z}} + \acute{\omega}^2\acute{z} = \frac{F_0}{m}\cos\Omega t, \tag{2.33}$$

where $\acute{\omega} = \sqrt{\frac{\acute{k}}{m}}$, and $\acute{k} = k - \frac{dF}{dz}$. By solving this differential equation and simplifying, the change in the resonant frequency due to the presence of the external force can be calculated to be

$$\Delta\omega_0 = \omega_0\left(\sqrt{1 - \frac{F'(z)}{k}} - 1\right). \tag{2.34}$$

This can further be simplified and approximated to the following:

$$\Delta\omega_0 \approx \frac{1}{2k}\frac{\partial F}{\partial z}\omega_0. \tag{2.35}$$

From this, it can be seen that as the distance between the sample and the tip changes (in the Z-axis), the forces (proportional to the forces seen in Figure 2.3) between the two will change significantly and thus substantially affect the resonant frequency. This will lead to higher resolutions because any change in the resonant frequency and its amplitude will be detected and amplified more than the simple motion of the cantilever moving along with the contour of the sample in contact mode.

2.4 Piezoelectric Crystals

The previous sections of this theory have given an explanation of the tip sample interactions during the approach and scanning processes. The following sections discuss some of the important mechanics involved in scanning samples. The piezoelectric effect is observed within certain crystalline materials that expand when an electric potential is applied to them. This concept of movement is critical for the implementation of an AFM as finite movements can be controlled by the slight adjustment of an electric potential

2.4.1 Piezoelectric Theory

Piezoelectric materials convert electric potential into mechanical motion. When the potential is applied to the two opposite sides of the material, the geometry is affected (see Figure 2.9).

In 1881, G. Lippman proposed that this was possible. Prior to Lippman, it was observed that certain materials produced an electric charge upon compression. Lippman hypothesized that this principle could be used in the opposite direction; that is, the potential will distort the crystal lattice, causing the piece to shrink in one direction and grow in the other.

From an electrical perspective, piezoelectric materials act similar to capacitors in that they are able to store as much as one hundred micro Farads on their surfaces [2]. Once charged, the piezoelectric material maintains the charge until it is dissipated by an electronic circuit.

These piezoelectric-materials can be formed into several different shapes in order to have more or less motion capabilities. There are two primary shapes that are formed for scientific use. The first of these would simply be a disk that gets longer but thinner when voltage is applied [2]. The other common shape that piezoelectric material is formed into is that of a hollow tube. Here, there are commonly four

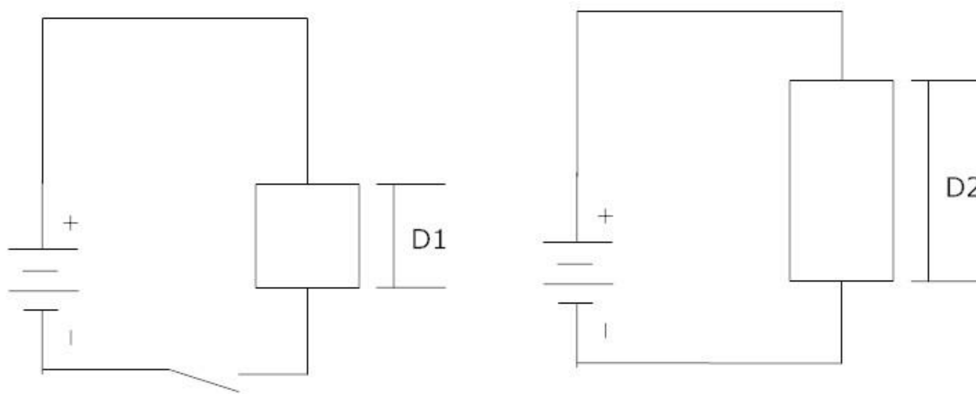

Figure 2.9. Expansion of a piezoelectric element. A piezoelectric element will expand when an electric potential is applied to the top and bottom of the material. The length will expand, but the overall volume will not change.

electrodes placed on the outside while the inside in one whole electrode. This configuration, as will be mentioned in the following section, gives the potential for much more motion and rigidity.

2.4.2 Approach and Scan Theory

The theorized plan for approaching and scanning the sample involves the use of piezoelectric elements and its theory. Consider the use of piezoelectric ceramic in the form of a cylindrical hollow tube (see Figure 2.10). The inside of the tube is set to ground while the outside is partitioned into four different parts each of which having a different possible electric potential. If all of the exterior leads are given the same voltage, then the thickness of the tube will either be contracted or expanded (depending on the voltage). As this occurs, the length of the sample will likewise expand or shrink in relation to the compression and expansion of the tube. If, on the other hand Y+'s potential is increased while Y-'s is reduced, the Y+ side of the cylinder will be compressed, becoming thinner (but taller as volume is conserved). The Y- side, on the other hand, will become thicker and, therefore, shorter. The whole net reaction to this will be the piezoelectric tube bending in the Y axis. The same thing can be done in the X axis. By using combinations of these three instances, the piezoelectric tube can be moved in any direction with a full range of motion.

The piezoelectric tubes yield a very effective method for moving a sample across the cantilever tip. To do so, three motions will be used: expansion and contraction, rocking movement, and the method known as the "stick-slip," in which the piezoelectric tube is able to move horizontally.

2.4.2.1 Expansion and contraction

As mentioned previously, if all four leads on the exterior of the piezoelectric tube are applied with the same voltage, the tube's shell will either contract or expand in thickness. As this occurs, the volume must be conserved, so the length of the tube will expand or shrink respectively (as can be seen in Figure 2.10 (a)).

2.4.2.2 Rocking motion

Rocking motion occurs when non-constant voltages are applied to the piezoelectric tube electrodes. A triangle wave voltage is appplied to the piezolectric tube. This triangle wave will cause the piezoelectric

tube to bend back and forth in relation to to its original position. In Figure 2.10 (b), if Y+ receives the voltage shown in the Voltage vs Time graph and Y- receives the opposite, the piezoelectric tube will move as shown. As V reaches the maximum in the red peak, the motion of the piezoelectric tube will reach a maximum along the red path. Conversely, as V reaches the minimum in the blue valley, the piezoelectric tube will reach a maximum along the blue path. This triangle wave would be repeated over a period of time causing the sample to scan back and forth along a line.

2.4.2.3 "Stick-slip"

The "stick-slip motion" is based on the rocking motion previously described. Instead of being a triangle wave, however, the wave applied is a saw-tooth. This means that instead of slowly decreasing after the peak, the voltage will immediately drop back down to 0. If the coefficient of friction between the end of the piezoelectric tube and the ground is small enough, then when the voltage suddenly drops the piezoelectric tube will slide over to where the top had moved (see Figure 2.10 (c)). This pattern can be repeated to move the walker indefinitely in the XY plane.

2.4.3 Error Sources

In an ideal situation, the piezoelectric tubes would change with direct linearity to the driving potential. Unfortunately though, there are two characteristics of piezoelectric materials that prevent the ideal from occurring: hysteresis and creep.

Hysteresis causes the material to maintain the shape that was formerly holding. This means that as the material expands it does in a nonlinear proportionality with the potential normally required. Conversely, as the material contracts in size, a similar phenomenon occurs. Both of these occurrences can be observed in the Figure. The characteristic known as creep occurs after a sudden, significant change occurs in the potential difference across the material. When this happens, the shape and dimensions of the piezoelectric material can continue to change despite the actual voltage remaining constant.

The combination of these two error sources create a potential problem for the scanning of a sample. They clearly can make significant issues for accurate measuring as well as causing scan times to be significantly longer. The current plans for the Houghton AFM do not involve a correction for this error.

One possible solution would be to have a feedback or feedforward control to monitor the error of hysteresis and creep .

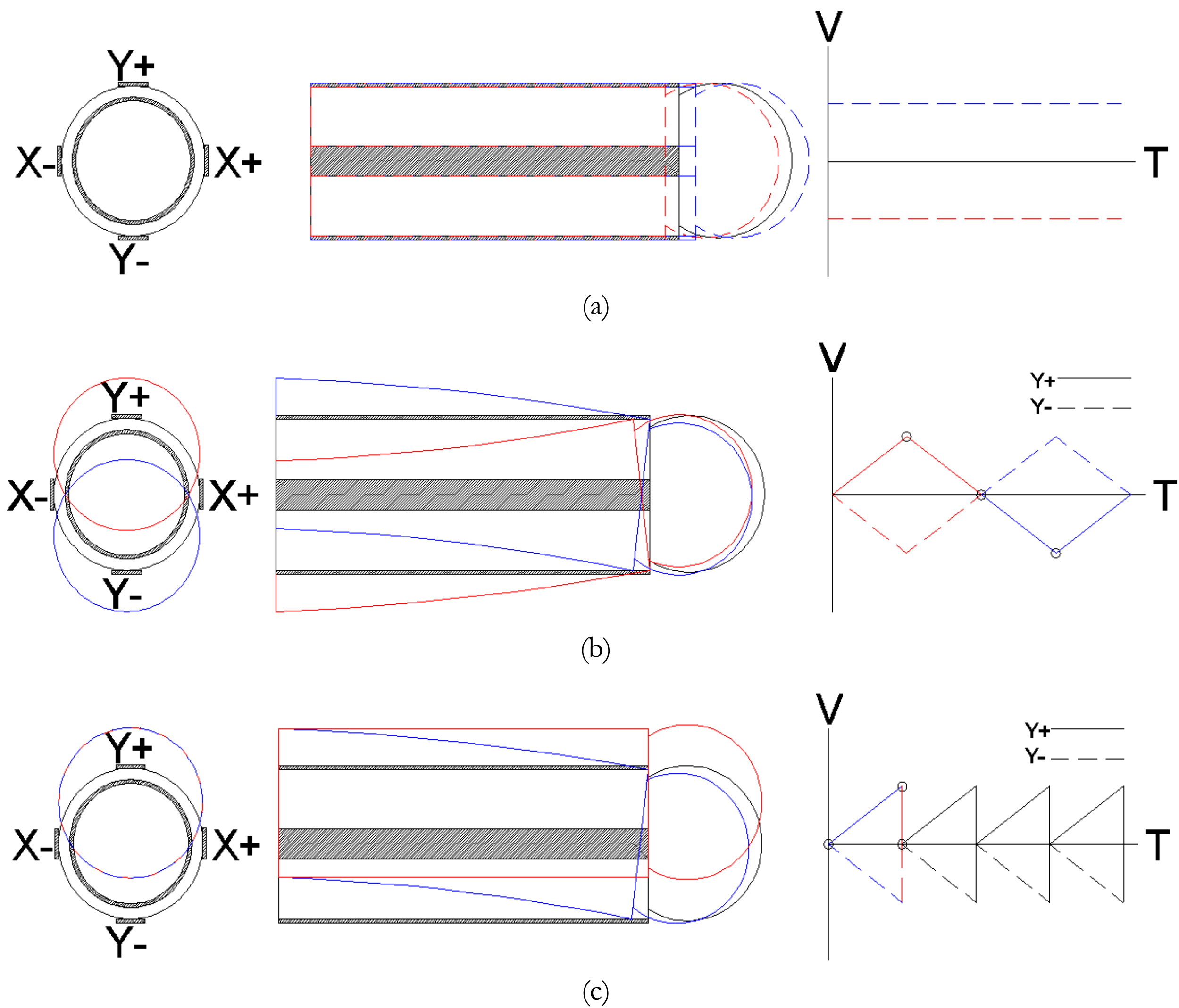

Figure 2.10. Schematics of the three movements required of the piezoelectric tubes. (a) describes the expansion/compression of the length of a tube if a constant voltage is applied to the exterior electrodes. (b) describes the motion of piezoelectric tube if two equal and opposite triangle waves are applied to opposite ends of the tube. (c) describes the motion that can occur if two equal and opposite saw tooth triangle waves are applied to the sides of the tubes and the piezoelectric tube is in contact with a surface that has a low coefficient of friction.

Chapter 3

AMF Apparatus

3.1 Overall Model

The Houghton College AFM (seen in Figure 3.1) will be based off of the AFM constructed in 1995 by Dai *et al* [8]. The initial intent for the Houghton AFM was to have a variable temperature capability during the scanning process. This plan, however, has been postponed since the variable temperature adds too many complications to the overall design of this AFM. Despite this, the Dai *et al.* model will still be used as an initial starting point. Modifications will be made to attempt to simplify the designs and potentially make a better AFM

3.2 Houghton Design

Some of the significant similarities between the Dai *et al.* [8] model and the eventual Houghton AFM will include the use of a laser system for detection and a "Johnny Walker" system for the movement of the sample for approach and scans. The sample and cantilever tip will be inverted in comparison to other models in an attempt to isolate the scanning apparatus (in order to reduce the interaction between the tip's high resonant frequency and the rest of the AFM). The walker will be controlled by a LabVIEW program and will operate on a platform that is isolated from the exterior surroundings by an eddy current damping spring oscillation system. A complete visualization of the Houghton AFM can be seen in Figure 3.1.

3.3 "Johnny Walker" Design

A "Johnny Walker" has been made for the purposes of scanning the sample in the Houghton AFM. It was created initially by Bethany Little [21]. The sample will be attached upside-down (so that the surface is facing downwards) to a ceramic post in the center of the piezoelectric tripod seen in Figure 3.1 and Figure 3.2. The walker will controll all of the movement the sample will make as it approaches and moves across the cantilever tip.

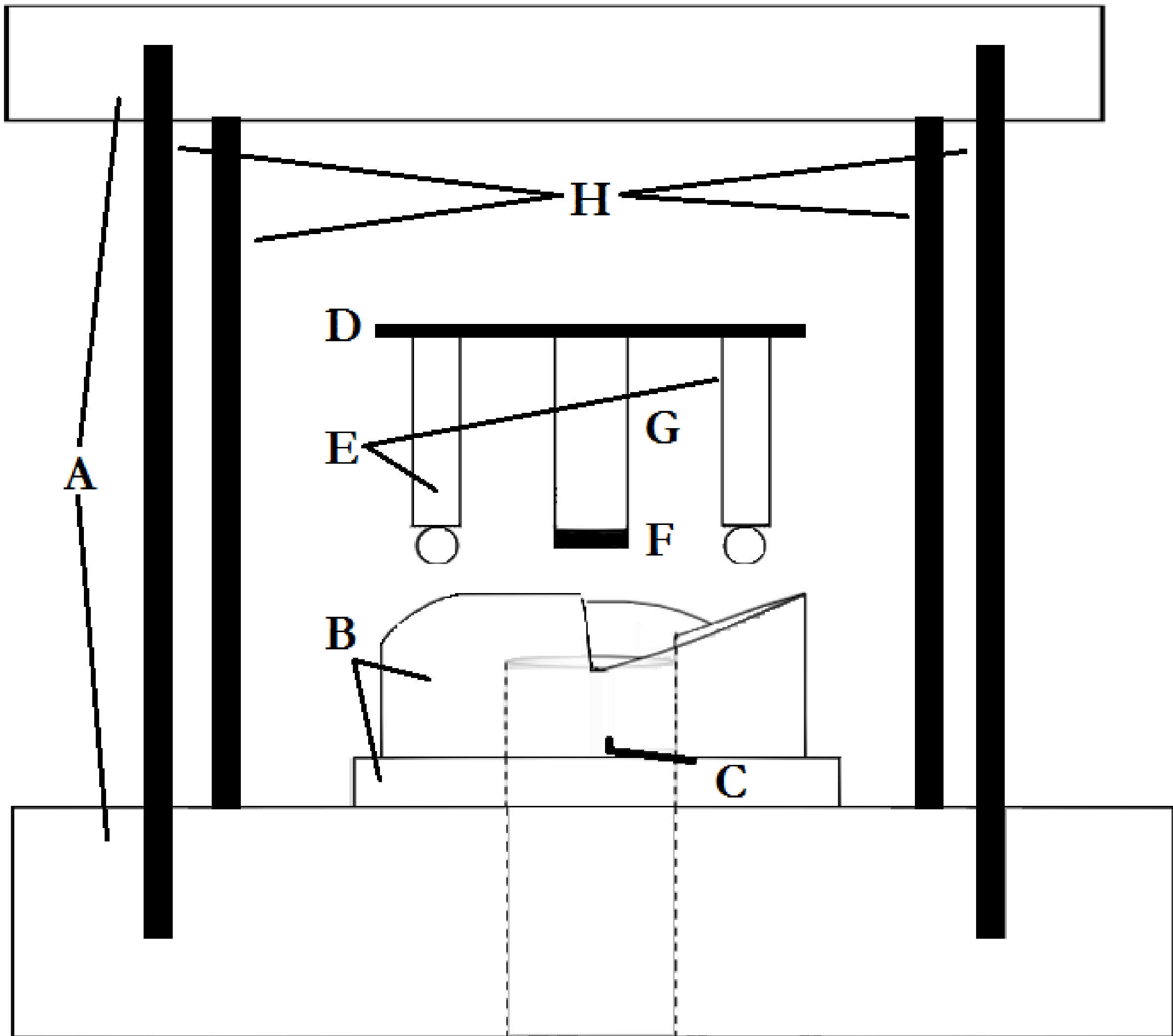

Figure 3.1. Schematic of the Houghton AFM. In this figure, (A) is the frame of the AFM, and is primarily made of aluminum. The ramp system (B) is made from aluminum rings and allows for the approach of the sample to the tip (C). The Sample is attached to a "Johnny Walker" (D) that consists of three piezoelectric tubes (E) (2 pictured) with sapphire balls attached on the bottom. At the center of these tubes, the sample (F) is attached to a ceramic post (G). This stage is suspended by four springs (H) that eliminate external resonant frequencies.

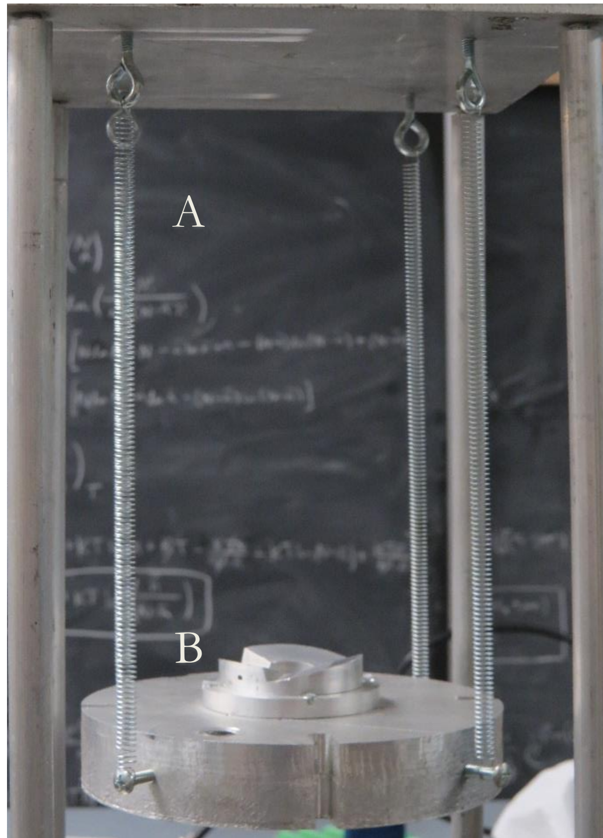

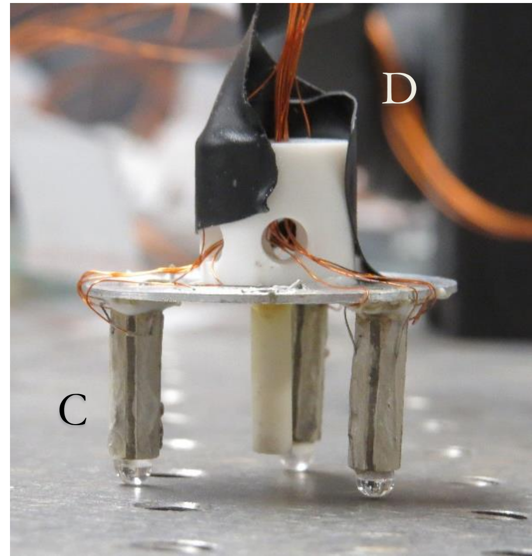

(a) (b)

Figure 3.2. Images of the Houghton AFM apparatus. (a) displays the main apparatus where the "Johnny Walker" (b) rests, approaches, and scan. "A" refers to the damping oscillation system, "B" refers the walker ramp and the platform that it resides on, "C" refers to the piezoelectric tubes and sapphire balls on their ends, and "D" shows the input wiring from the computer.

3.3.1 Sample Movement: Approach

The walker and sample unit will approach the cantilever tip using the stick-slip method of approach. It will move along a circular inclination that is made up of three individual ramps. Each ramp has a slope steepness of approximately 10°. The walker's piezoelectric legs rest on each ramp. When a saw-tooth voltage wave powers the piezoelectric tubes in the proper timing and magnitude, the three tubes will move in synchronization and move down the ramp. An optical laser system will be used to ensure that the sample and tip do not get damaged as the sample nears the tip. A program was written [12] to check

before each step is made to make sure that the sample is not too close to the tip before continuing to step down.

Additionally, the walker can also move along the XY plane using this method in order to get a rough sample position that can be further refined.

Fine tuning of the sample position can be achieved by applying a potential to the tubes that causes them to bend (see Figure 3.3). This causes them to move without initiating the stick-slip process (a much bigger movement than the slight bending). This will not only allow for movement in the Z-direction, but it will also allow for the fine tuning of position in the XY plane for a given scan. This movement is achieved the same way as the scanning motion.

3.3.2 Sample Movement: Scanning

Once the sample has been put in the approximately correct location for the scan, a different method of movement must be implemented. This method will be used to fine tune the sample's position relative to the cantilever tip and also to scan the sample across the tip.

The method for fine tuning and scanning must be broken up into three different sections: X, Y, and Z directions. The simplest of these three is controlling the height (Z-component) movement. This is measured by the optical laser feedback loop that detects when the tip is close to being in contact with the sample. The movement in the Z-direction is controlled by putting different potentials on the inner lead of each piezoelectric tube. A lower voltage on the inner electrodes will result in motion up, whereas a higher voltage will cause the sample to come closer to the cantilever tip.

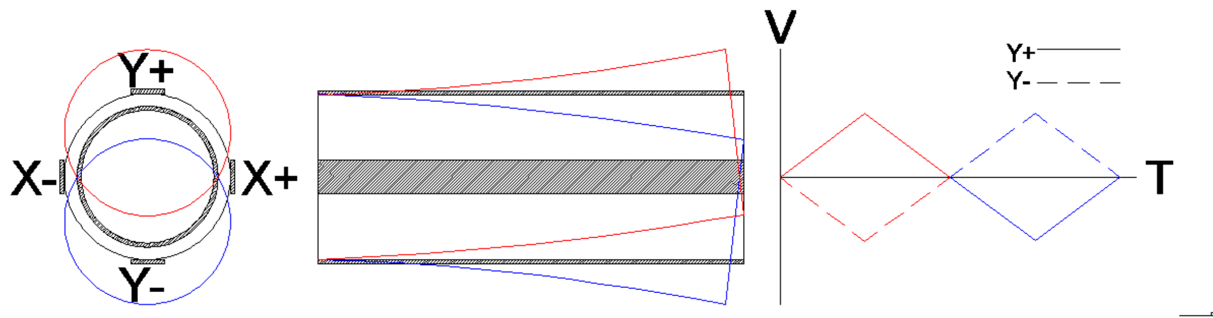

Figure 3.3. Schematic of the piezoelectric tube movement under a triangle voltage. If the piezoelectric tubes have two equal but opposite triangle waveforms applied to the opposite electrodes, the following ensues. As Y+ receives the solid line voltage and Y- receives the opposite in the dashes line seen the voltage vs time graph, the piezoelectric tube will move as shown. As V reaches the top of the red peaks, the motion of the piezoelectric tube will reach a maximum along the red path. Conversely, as V reaches the top of the blue tips, the piezoelectric tube will reach a maximum along the blue path. This motion, if repeated will cause a rocking motion that will move the sample across the tip

To scan across the image and create a topographic map, a triangle wave voltage is appplied to the piezolectric legs. This triangle wave will cause the piezoelectric tube to bend back and forth in relation to to its original position. Figure 3.3 displays how this movement would be realized for useful purposes. As Y+ receives the voltage shown in the V-T graph and Y- receives the opposite, the piezoelectric tube will move as shown. As V reaches the maximum in the red peak, the motion of the piezoelectric tube will reach a maximum along the red path. Conversely, as V reaches the minimum in the blue valley, the piezoelectric tube will reach a maximum along the blue path. This triangle wave would be repeated over a period of time causing the sample to scan back and forth along a line. To scan an entire sample, a slower triangle wave would be out onto the adjacent leads in similar fashion (e.g. in Figure 3.3 a smaller frequency of the triangle wave would be sent to the X+ and the opposite to X-). This slower triangle wave will cause the sample to be scanned in a series of lines, that is, the sample will move across the tip in the faster waves direction and then it will move in the slower frequency's and repeat. The number of lines in the image can be found from the two frequencies:

$$n = \frac{f_x}{f_y} \tag{3.1}$$

where f_x and f_y are the frequencies of the waves applied.

3.4 Electronic Circuitry

An electronic circuit has been created to control the movement of the sample across the tip via a computer. This circuit has been split into two separate sections: the digital to analog portion and the voltage amplification circuit for the piezoelectric tubes.

3.4.1 Digital to Analog Circuitry

The piezoelectric tubes on the "Johnny Walker" require a range of voltage from 0 to 2000 V. The first thing that must be done to control these piezoelectric tubes is convert the digital signal from the computer into an analog voltage. An NI 6221 (68 pin) PCI board will be used to output directly from the computer. The signal generated from this board will then go directly into an eight bit, eight channel TLC5628C digital to analog converter (DAC) chip. From there an analog signal will go to five EMCO C20 miniature regulated HV power supplies (AMP) – see Figure 3.4. Data is read into a TLC8628C Octal 8 bit DAC in serial and is captured with the use of a clock and R/W pulse. The data is then

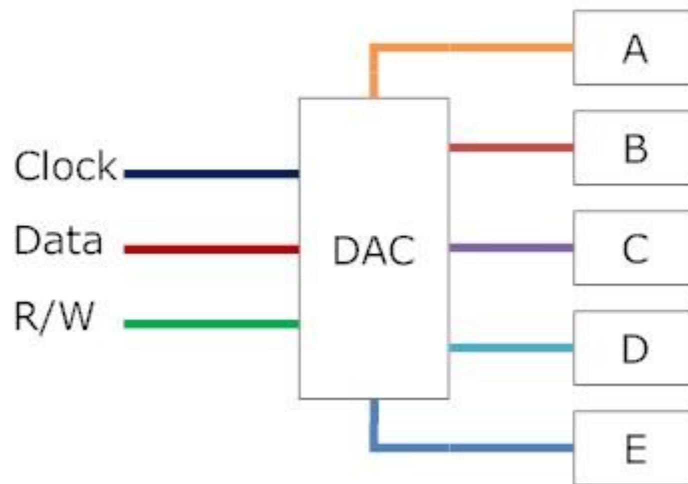

Figure 3.4. Schematic of the DAC circuitry. Data is read into a TLC8628C Octal 8 bit DAC in serial and is captured with the use of a clock and R/W pulse. The data is then partitioned into the designated DAC output (one of 8 possible outputs). These outputs then are connected to 5 EMCO miniature, regulated HV power supplies (A-E)

partitioned into the designated DAC output (one of 8 possible outputs). These outputs then are connected to 5 EMCO miniature, regulated HV power supplies (A-E). The signal includes three bits to designate which output, one bit to designate the range of the output voltage, and eight bits that make up the actual output voltage. For the purposes of the Houghton AFM, only five of the eight channels will be required. The data comes in as serial and is in phase with the clock pulse. An R/W pulse is used to collect the signal and send it to the designated output. Figure 3.5 displays the timing diagram for the three inputs into the DAC. It is important to note that for every downward clock pulse one bit of data is read into the DAC. Once one string of data is read into the DAC, the clock stops and the R/W pulses. This process is then repeated for the next set of data. This entire process will occur five times (since five analog outputs are required), forming a set. The set will then start over, updating the output values.

The EMCO miniature regulated HV power supplies recieve a voltage between 0 and 5 VDC at up to 1 Watt and output a voltage proportional to the input but on a scale of 0 to 2000 VDC at up to 1 Watt. The power supplies require grounding and a 12 to 15 VDC power supply.

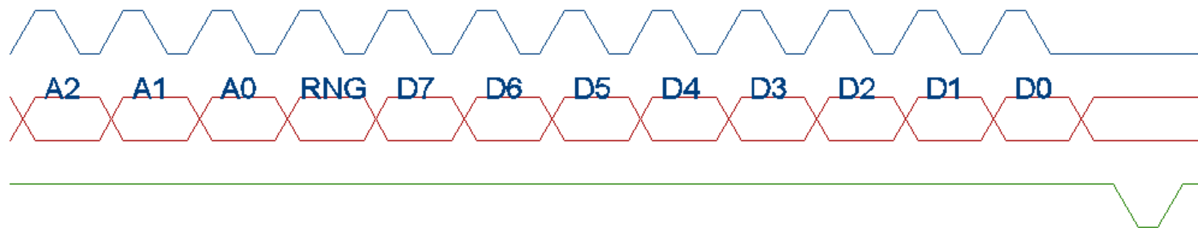

Figure 3.5. Timing diagram of the TLC5628C DAC. For every downward clock pulse (blue) one bit of data (red) is read into the DAC. Once one string of data is read into the DAC, the clock stops and the R/W pulses (green). This process is then repeated for the next set of data. This entire process will occur five times (since five analog outputs are required), forming a set. The set will then start over, updating the output values.

3.4.2 Piezoelectric Circuitry

After the EMCO miniature regulated HV power supplies amplify the output from the computer the voltage is put through two individual circuits simultaneously before reaching the piezoelectric tubes – a circuit for approach and a circuit for scanning the sample. The two circuits then go through a switch that will be manually adjusted by the operator to either move the sample into position or begin scanning.

The approach circuit is much more complicated than the scanning circuitry as the AMPS must be adjusted to account for the circular motion that the walker requires to descend towards the cantilever tip. Figure 3.6 displays the geometry of the Johnny Walker. The three piezoelectric tubes are located at the points of an equilateral triangle. In order to get tangential movement it must be broken up into components in the XY axis as shown. By breaking this up, the components of the movement form a 30-60-90 triangle (from the basic geometry). If V_B is the voltage required for the hypotenuse of the 30-

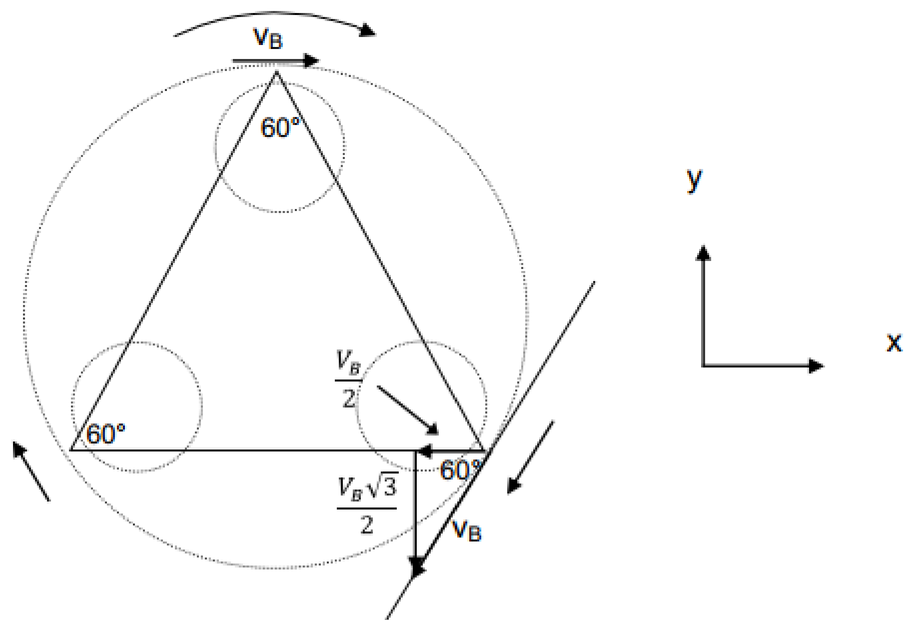

Figure 3.6. Diagram showing the geometry calculations for the approach circuit. Here is can be seen that the piezoelectric tubes are positioned on an equilateral triangle. In order to attain a tangential velocity v_b on all of the tubes, simple geometry must be used.

60-90 triangle, the two other sides of the triangle (and thus the components) can be calculated through the use of

$$V_1 = V_b \sin\frac{3\pi}{2} \text{ and } V_2 = V_b \cos\frac{3\pi}{2} \qquad (3.2)$$

From this, it can be seen that if the voltage from AMP B is adjusted by factors of $\frac{1}{2}$ and $\frac{\sqrt{3}}{2}$, then the walker will move in a circular pattern down the ramp [12]. The electrodes on each of the respective piezoelectric tubes are connected to the specifically noted amplifiers in Figure 3.6 and Figure 3.7to move the walker.

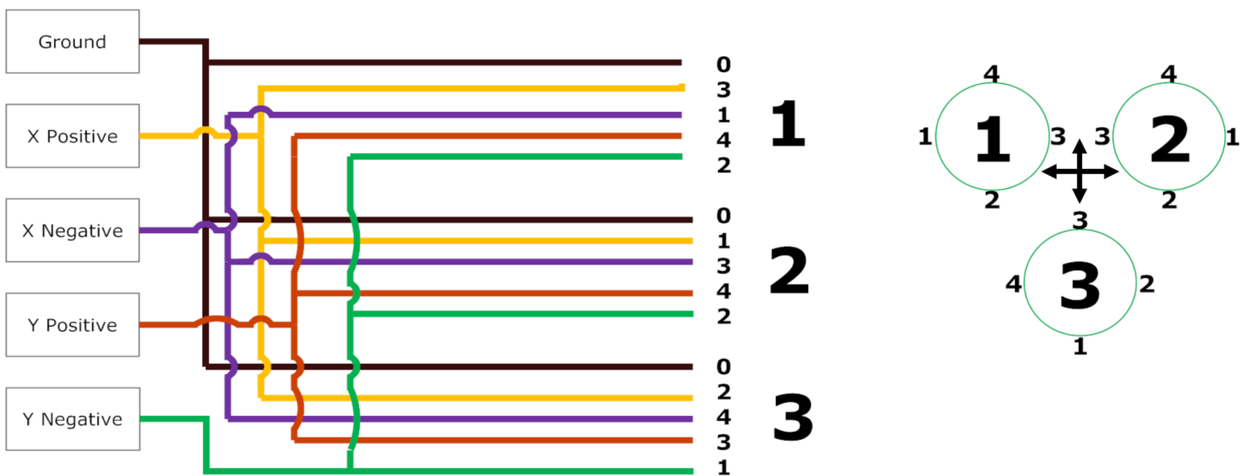

Figure 3.7. Scanning Circuitry. The scanning circuitry uses 5 voltage amplifiers (labeled Ground (A), X Positive (B), X Negative (C), Y Positive (D), and Y negative (E)). The output from these amplifiers are connected to the piezoelectric tubes of the "Johnny Walker" and control movement in a gird like motion.

The scanning circuitry is much simpler as circular movement is not required to scan the sample across the cantilever tip. Figure 3.7 and 8 display how the amplifiers are connected to the piezoelectric tubes. It should be noted that "Ground" in Figure 3.7 is equivalent to A in Figure 3.8, X Positive to B, and so on. This circuit, coupled with the triangle wave voltage output from the computer, will effectively move the sample in a grid like motion across the cantilever tip, causing it to create a topographic map of the sample.

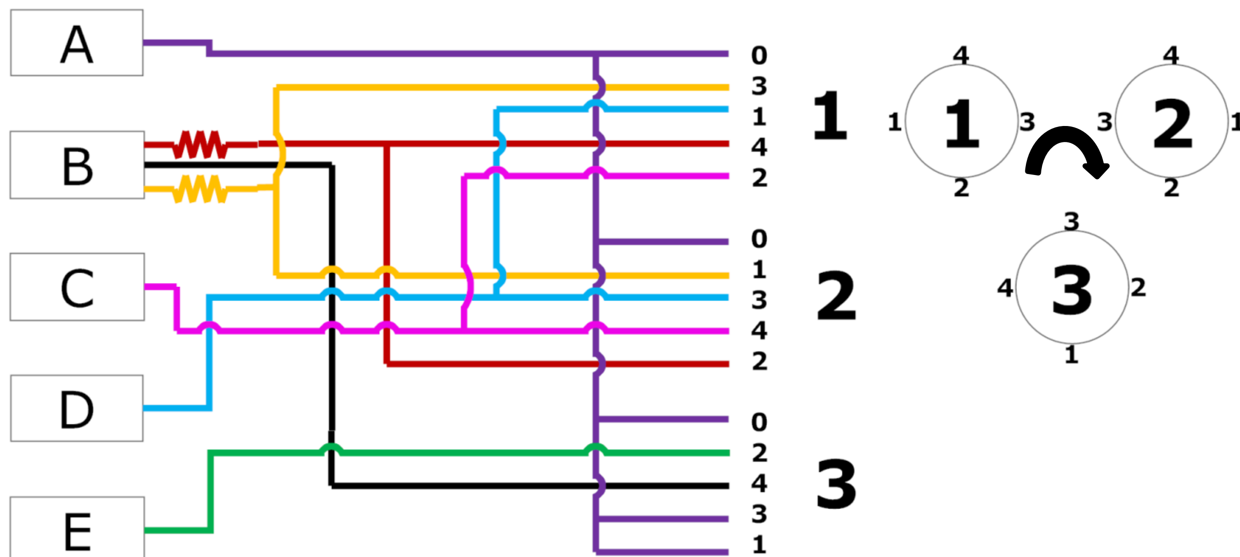

Figure 3.8. Approach Circuitry. The approach circuitry consists of 5 voltage amplifiers (A-E) which are then connected to the "Johnny Walker" via the leads on the three piezoelectric tubes. The amplifications from B go through additional circuitry to obtain 3 different voltages: B (black), $\frac{1}{2}$B (red), and $\frac{\sqrt{3}}{2}$B (yellow). This allows for the walker to rotate in a circular pattern.

3.5 LabVIEW Program

The programs that control the "Johnny Walker" and scan the sample were created and operate in LabVIEW 8.2 (student edition). The programs will drive the piezoelectric tubes to scan and move the sample, read in the laser detection system, and create topographic maps of the sample surface. Currently, the only program to be completed in full is the piezoelectric controlling output program.

3.5.1 Output Program

The output program is shown in Figure 3.9 through Figure 3.12. These figures illustrate the processes involved in controlling the piezoelectric tubes. The current program begins with a "while loop" that creates a positive and negative saw tooth wave. These waves are essentially step functions that, after a

specific time interval, increase or decrease by an amount the user designates (see Figure 3.9). At each increment and decrement of the waves, the while loop pauses to output this value to the DACs. When it has been outputted, the while loop continues. Once the maximum and minimum are reached for each wave function, the function resets to the original value and begins the saw tooth pattern again.

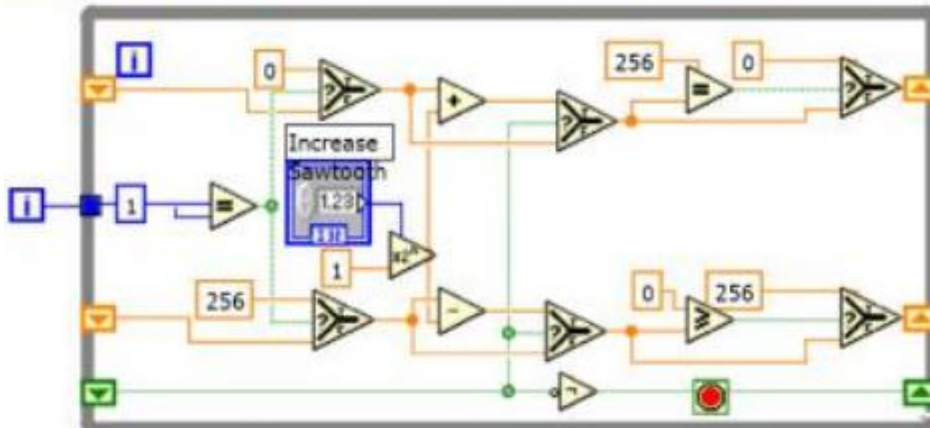

Figure 3.9. Diagram of the saw tooth wave creation. Here, the user designates the step size of the saw tooth waves (both positive and negative). This value then is subtracted or added from the initial values of the waves (for the negative wave, 256, and for the positive wave, 0). The value is then taken from this loop and the loop ends until the outer loop also ends. Then, the new value replaces the initial values and this process repeats until 0 becomes 256 and 256 becomes 0. Once this occurs the entire process is repeated.

The next part of the program decides what will be outputted to the individual DACs (as seen in Figure 3.9). Here, the two saw tooth waves from Figure 3.9 are brought in and put into a choosing scheme for the user. Looking at DAC 1, if the user chooses 1 on the interface, one of the saw tooth waves is chosen as the output. If 2 is chosen, the other wave is chosen. If 3 is chosen, however, a constant value designated by the user will be set as the output. The output from this choice is then sent through a number to array converter along with the address for that particular DAC output in the TLC8628C. These are all combined into one array that is not ordered properly for the output. Both positive and negative saw tooth wave values are sent to the selection mechanism. This is used to select which option will go to the DAC output. In addition to these waves, a constant voltage can be chosen to be the output to the DAC. This current setup is used for testing the program and causing the walker to move. Further programming will need to be done in order to cause the walker to approach and scan

properly. Once an option has been selected by the user for each DAC, the values are converted into binary and put into an array of zeroes with the output destinations. The strings that are input replace the necessary zeroes – anything beyond the strings remains zero. This array is not in the correct order for the final output (since the chip needs to have a serial output). At this point, the output is as follows:

$$x_{10}\text{-}x_{11}\text{-}x_{12}\text{-}0\text{-}0\text{-}0\text{-}0\text{-}0\text{-}0\text{-}0\text{-}0\text{-}0\ldots$$
$$d_{10}\text{-}d_{11}\text{-}d_{12}\text{-}d_{13}\text{-}d_{14}\text{-}d_{15}\text{-}d_{16}\text{-}d_{17}\text{-}0\text{-}0\ldots$$
$$x_{20}\text{-}x_{21}\text{-}x_{22}\text{-}0\text{-}0\text{-}0\text{-}0\text{-}0\text{-}0\text{-}0\text{-}0\text{-}0\ldots$$
$$d_{20}\text{-}d_{21}\text{-}d_{22}\text{-}d_{23}\text{-}d_{24}\text{-}d_{25}\text{-}d_{26}\text{-}d_{27}\text{-}0\text{-}0\ldots$$
etc.

where x_{nn} is the address of the output on the DAC chip and d_{nn} is the data bit for that address. Once the array is in this form, it must be transformed into the following form:

$$x_{12}\text{-}x_{11}\text{-}x_{10}\text{-rng-}d_{17}\text{-}d_{16}\text{-}d_{15}\text{-}d_{14}\text{-}d_{13}\text{-}d_{12}\text{-}d_{11}\text{-}d_{10}\text{-}0\text{-}0\text{-}x_{22}\text{-}x_{21}\text{-}x_{20}\text{-rng-}d_{27}\text{-}d_{26}\text{-}d_{25}\text{-}d_{24}\text{-}d_{23}\text{-}d_{22}\text{-}d_{21}\text{-}d_{20}\text{-}0\text{-}0\ldots \text{ etc.}$$

where rng is a 0 or a 1 the range of the output (i.e. the scale of the output). 0 denotes a scale of 0 to 5 VDC and 1 denotes a scale of 0 to 10 VDC. Since the AMPs require a range of 0 to 5 VDC as the input voltage, the rng will be 0 for all cases. Since there are additional zeroes past the actual data, the process of converting to a serial output is slightly more complicated. To transform, this array is sent into a while loop to reorder. This is done by using premade arrays of numbers to call each value at the proper time (See Figure 3.11). In Figure 3.11 (a), the initial array is connected into an index array function where the indexing parameters are 2 arrays of numbers that are called by the iterations of the while loop. By doing this, the array will be reordered into the proper format, creating a serial line of the array for a one step increment of time for each DAC output (A through E). Figure 3.11 (b) displays the arrays used to create the timing for the clock and R/W for the chip. Since the clock pauses after one string of data finishes and while the R/W pulses, it is necessary to create an array for each so that they are in sync with the data

stream. Now, there is a set of 3 outputs that match with the timing required for the DAC TLC5628C chip shown in Figure 3.5

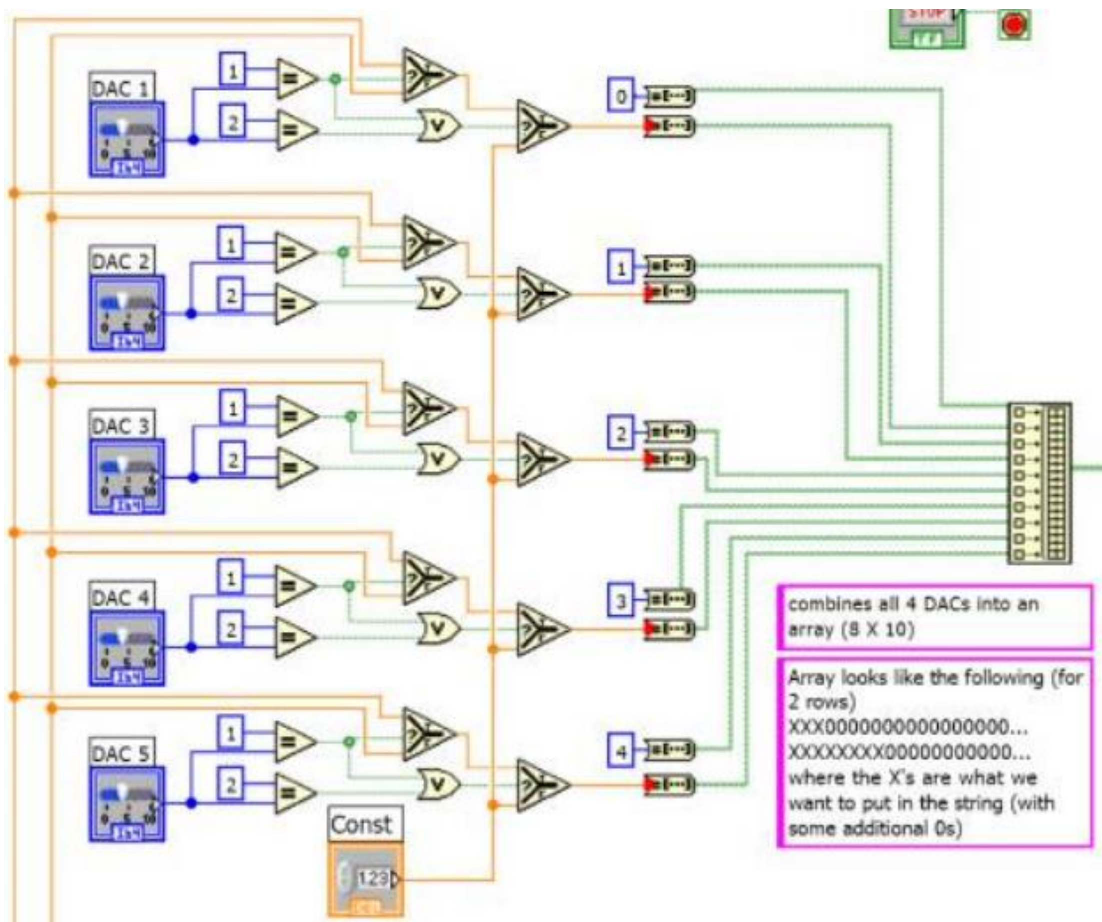

Figure 3.10. Diagram that displays the process of choosing what is outputted to each individual DAC and the conversion to binary. Here, the two saw tooth waves from Figure 3.8 are brought in and put into a choosing scheme for the user. Looking at DAC 1, if the user chooses 1 on the interface, one of the saw tooth waves is chosen as the output. If 2 is chosen, the other wave is chosen. If 3 is chosen, however, a constant value designated by the user will be set as the output. The output from this choice is then sent through a number to array converter along with the address for that particular DAC output in the TLC8628C. These are all combined into one array that is not ordered properly for the output.

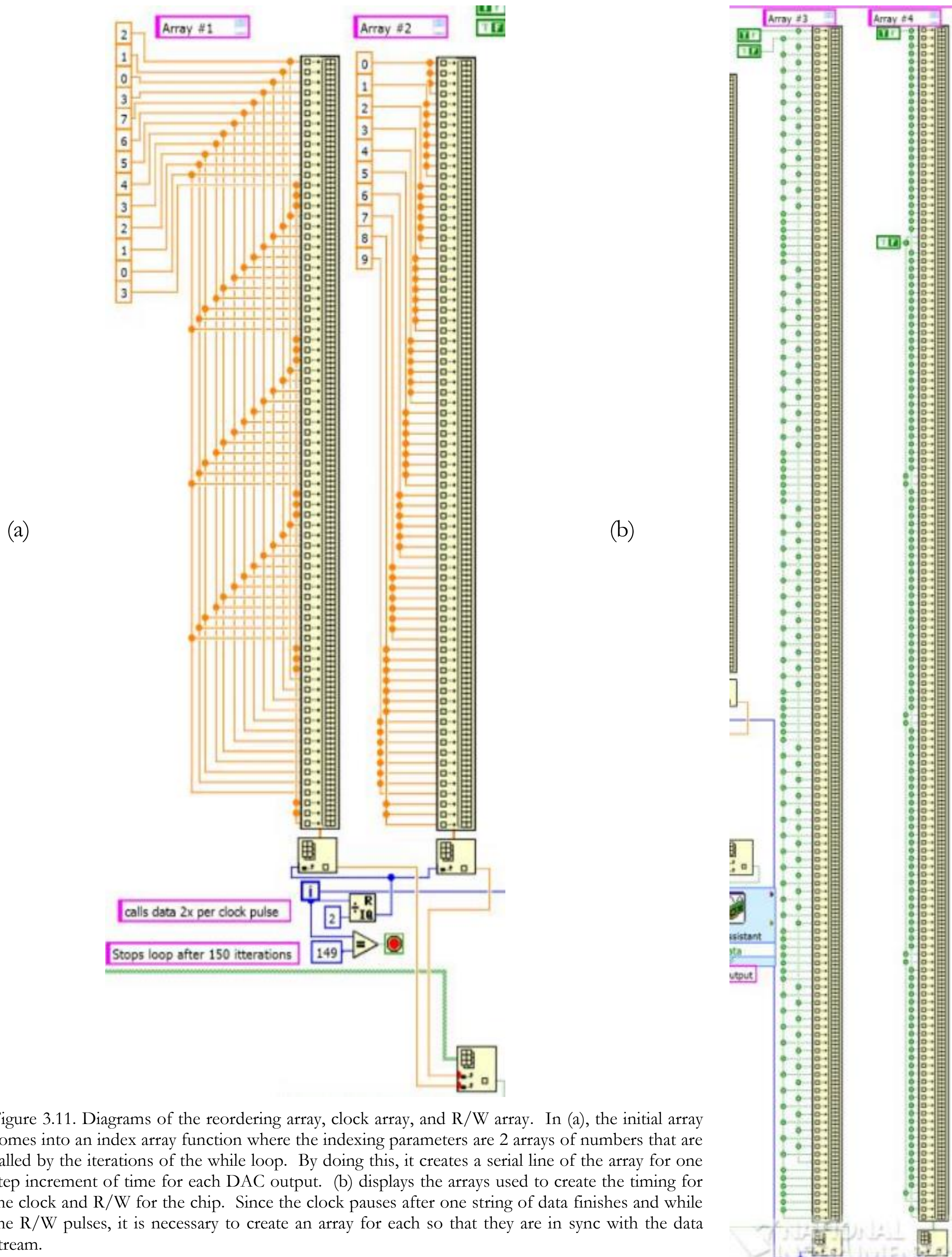

Figure 3.11. Diagrams of the reordering array, clock array, and R/W array. In (a), the initial array comes into an index array function where the indexing parameters are 2 arrays of numbers that are called by the iterations of the while loop. By doing this, it creates a serial line of the array for one step increment of time for each DAC output. (b) displays the arrays used to create the timing for the clock and R/W for the chip. Since the clock pauses after one string of data finishes and while the R/W pulses, it is necessary to create an array for each so that they are in sync with the data stream.

Now that the outputs have been created in LabVIEW, they are ready to be exported to the DAC. This is done by using the DAQ assistant function in LabVIEW. This assistant sends the data to the PCI board in the computer which is then connected to the DAC chip. The programming aspect of this can be seen in Figure 3.12 (a) and (b). The analog output (a) consists of two outputs that must be 5 VDC – one is to power the DAC, the other is a reference voltage for the DAC. The digital output is pictured in (b). The clock, data load (R/W pulse) and LDAC (required, but held to LOW) are outputs to the DAC.

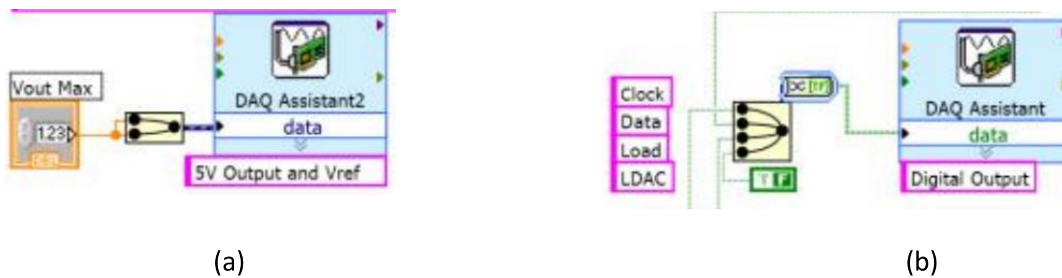

Figure 3.12. Diagrams displaying the analog and digital outputs of the program. (a) displays the analog output of the PCI board. There are two outputs that must be 5 VDC – one is to power the DAC, the other is a reference voltage for the DAC. The digital output is pictured in (b). The clock, data load (R/W pulse) and LDAC (required, but held to LOW) are outputs to the DAC.

3.6 Implementation

With all of this having been completed, here is a brief synopsis of how each component mentioned will be combined together to form a functional AFM. Observe Figure 3.13. The computer sends a digital signal through the PCI chip to the DAC which converts the digital signal and sends analog signals to 5 separate voltage amplifiers. These amplifications go through two separate circuits (1 for scanning and 1 for approaching the sample) before going to a switch. The switch controls which process will occur (scanning or approaching). Once through the switch, the signal goes directly to the piezoelectric tubes, which move the sample via the "Johnny Walker."

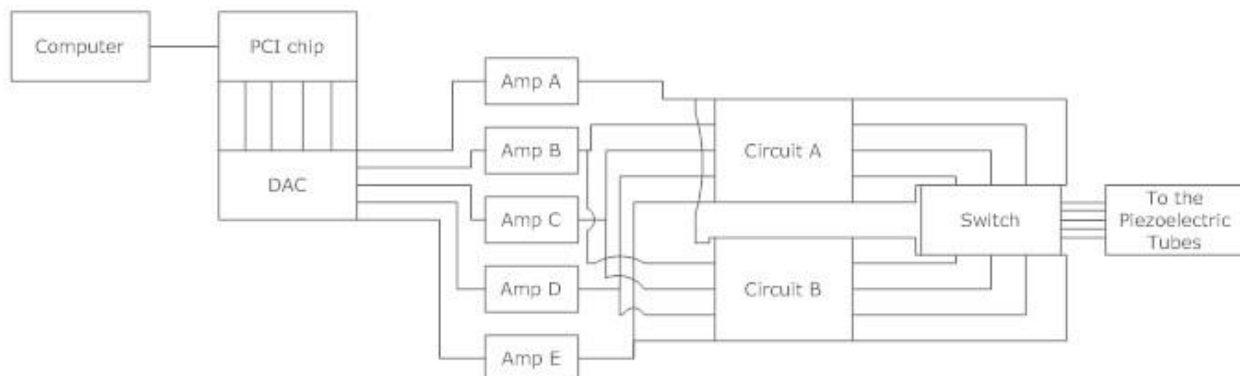

Figure 3.13. Schematic of the entire electrical circuit for moving the "Johnny Walker" and scanning the samples via the piezoelectric tubes. The computer sends a digital signal through the PCI chip to the DAC which converts the digital signal and sends analog signals to 5 separate voltage amplifiers. These amplifications go through two separate circuits (1 for scanning and1 for approaching the sample) before going to a switch. The switch controls which process will occur (scanning or approaching). Once through the switch, the signal goes directly to the piezoelectric tubes and move the sample via the "Johnny Walker."

Chapter 4

RESULTS AND CONCLUSION

4.1 Current Status

Thus far, the status of the Houghton AFM remains unfinished, though significant steps have been taken for its completion. A working output module has been designed, constructed, and tested successfully. This, coupled with the main approach, scan and data collection programs will complete a fully functional program that can operate the AFM. Additionally, the "Johnny Walker" has been constructed and been attached to the output module. It is currently in the testing phases of the construction process.

4.2 Future Work

Much more work that to be done before the Houghton AFM is fully functional. A laser optical system must be created and working before any data can be collected. Also, the multiple programs that have been created must be made compatible with each other. The scanning and approach module must be in sync with the output module and work alongside the data collection unit. To do this, a separate program will need to be created to control all of these sub programs and make them run in unison.

Different parts of the AFM will also need to be assembled. This will include the attachment of the optics system, eddy current damping system, cantilever, and various electronic circuits that move and control parts of the machine.

Testing and calibrating will also need to be done to have a functional microscope. Calibration of the "Johnny Walker's" movements along with the accuracy of the output modules voltages will need to be conducted. The accuracy of the optical system must also be measured. Finally, testing of the overall machine will need to be completed before scans will be taken.

4.3 Conclusion

The Atomic Force Microscope is an important tool for the use of the Houghton College Physics Department. It will allow for the study of thin films to be better researched at Houghton. The Houghton AFM will, in its completed state, be fully equipped with a "Johnny Walker" sample holder, whose movements are detected by a laser deflection optics system. The walker's movements are controlled by piezoelectric tubes and will be controlled by a LabVIEW program.

[1] G. Binnig et al, Physical Review Letters, **56**, 9 (1986).

[2] P. E. West, *Introduction to Atomic Force Microscopy: Theory, Practice, Applications*, http://bitc2-preview.sr.unh.edu/TRC/REFERENCES/AFM/AFM_TheoryPracticeApplications_TEXT.pdf, (5 May 2014).

[3] D. J. Whitehouse, *Handbook of Surface and Nanotechnology* (CRC Press, 2011), p. 256.

[4] Young et al, Review of Scientific Instruments, **43**, 999 (1972).

[5] Binnig et al, Surface Science **126**, 236-244 (1983).

[6] K. vanstreels et al, J. Mater. Res. **23**, 3 (2008).

[7] T. Yoshitake et al, Applied Surface Science **141**, 129-137 (1999).

[8] B. Gautier et al., Applied Surface Science, **217**, 108-117 (2003).

[9] J. D. Mertzlufft, B.S. Thesis, Houghton College at Houghton, 2013.

[10] T. G. Reynolds, B.S. Thesis, Houghton College at Houghton, 2013.

[11] A. C. Evans, B.S. Thesis, Houghton College at Houghton, 2013.

[12] Q. Dai et. al., Rev. Sci. Instrum. **66**, 5266 (1995).

[13] M.H. Mahdavi et. al., Ultramicroscopy **109**, 54 (2008).

[14] V.J. Morris et al, *Atomic Force Microscopy for Biologists* (Imperial College Press, 2010), p. 44.

[15] S-w. Lee, et al., Colloids and Surfaces A: Physicochem. Eng. Aspects **204**, 43 (2002).

[16] D. Sarid, *Scanning Force Microscopy: With Applications to Electric, Magnetic, and Atomic Forces*, (Oxford University Press, 1991), p. 187.

[17] H.C. Hamaker, Physica, **4**, 1058 (1937).

[18] D. Sarid, *Scanning Force Microscopy: With Applications to Electric, Magnetic, and Atomic Forces*, (Oxford University Press, 1991), p. 189.

[19] W. N. Sharpe, W. N. Sharpe Jr., *Springer Handbook of Experimental Solid Mechanics,* (Springer Science+Buisness Media LLC, 2008), p. 425-426.

[20] NT-MTD "Cantilever Linear Oscilations" *SPM Basics*, http://www.ntmdt.com/spm-basics/view/linear-oscillations, (5 May 2014).

[21] B. Little, B.S. Thesis, Houghton College at Houghton, 2009.